8-2-2011

Electrochemical Synthesis of Single Crystal Metal Nanowires

Nan Li
University of Connecticut - Storrs, nan.li@uconn.edu

Electrochemical Synthesis of Single Crystal Metal Nanowires

Nan Li

B.S., Dalian University of Technology, 2009

A Thesis

Submitted in Partial Fulfillment of the

Requirement for the Degree of

Master of Science

at the

University of Connecticut

2011

APPROVAL PAGE

Master of Science Thesis

Electrochemical Synthesis of Single Crystal Metal Nanowires

Presented by

Nan Li, B.S.

Major Advisor _____
Brian G. Willis

Associate Advisor _____
Yu Lei

Associate Advisor _____
Puxian Gao

University of Connecticut

2011

ACKNOWLEDGEMENTS

This thesis cannot work successfully without the help of many people.

First of all, I would like to sincerely thank my advisor, Dr. Brian G. Willis, for all his guidance, patience, support and remarkable ideas contributed to my work.

Thanks to Dr. Yu Lei from Uconn Chemical Engineering and Dr. Puxian Gao from Uconn Material Science Engineering for accepting to be in my Advisory Committee. Specially, thanks to Dr. Lei Yu for using the potentiostat and Dr. Puxian Gao for using the sputter coater for my experiments.

Thanks go to Dr. Lichun Zhang and Dr. Roger A. Ristau at the Microscopy Laboratory of Uconn Institute of Material Science for their aid with the operations of SEM and TEM, and the patience of expaining all my questions. I also thank Dr. Jack Gromek for getting me nice sets of data in XRD measurements, and Kuo-Ting Liao for helping me use the sputter coater.

Thanks to my colleages, Dr. Yu Ding, Liang Su, Wenzhao Jia, Ying Wang, Han Wang and Xiaoqiang Jiang for the useful dicussions.

Further thanks to the National Science Foundation for supportting this project.

All my love and thanks to my parents for being there for me all the time.

Finally, love and thanks to Michael, for your support by accompanying and helping me go through the thesis again and again.

TABLE OF CONTENTS

LIST OF TABLES

LIST OF FIGURES

ABSTRACT

Electrodeposition is an efficient and economical approach for template synthesis of one-dimensional (1D) nanostructured materials. Based on the porous membranes as templates during electrodeposition, metallic nanowires, nanorods, and nanotubes can overcome the geometrical restrictions to be inserted into the nanometric recesses with both diameter and length well controlled by tuning the size and thickness of the templates.

In this work, the morphology, growth rate and texture of copper nanowires prepared with templates were investigated by the controlled parameters in various experiments. Cu nanowire arrays with preferential orientations can be successfully synthesized into the Anodic Aluminum Oxide (AAO) templates with optimized electrodepositing conditions at room temperature. The nanowires embedded in AAO were released and dispersed on Si/SiO_2 wafer for further observation and analysis in the preliminary studies. The morphology of the copper nanowires has been characterized by scanning electron microscopy (SEM), demonstrating the high density of nanowires grown into the pores of AAO. The chemical composition and crystalline structures of copper nanowires were analyzed by Energy-dispersive X-ray spectroscopy (EDS), X-ray diffraction (XRD), and Transmission Electron Microscopy (TEM).

Both potential and current were used as controlled variables during electrodeposition. Also, the influences of deposition time, concentration of $CuSO_4$ H_2O in the electrolyte and pH value on morphology and crystalline structure of copper nanowires were investigated. Results show that the

diameters of nanowires are 200 nm, same as the pore size of the templates. The lengths of nanowires are positively correlated with the deposition time and the growth rate of nanowires is strongly affected by the applied potential and concentration of the electrolyte. Characterizations of XRD and TEM proved that (220) is the preferential orientation of copper nanowires when lower current density was selected for electrodeposition with a galvanostatic experiment. The orientation obtained was the same as the preferential orientation of nanowires prepared in an electrolyte with higher pH using a potentiostatic technique. Moreover, a different preferred growth direction of [200] was identified when a less negative applied potential was employed, as well as increasing the current density in a certain range. The nucleation-growth mechanism of nanowires during electrodeposition was systematically investigated and results concerning preferred orientations were compared with previous studies. Overall, we demonstrated how growth rate and preferred orientations could be controlled using electrodeposition to prepare copper nanowires. Extension of the methods for synthesizing other nanowires is also discussed. This approach may contribute to applications that require single-crystal metallic nanowires along a cubic axis direction, e.g. electronic tunneling devices.

Chapter 1 INTRODUCTION

1.1 Metallic Nanowires

Nanostructured materials have attracted considerable attention in the past two decades because of their unique properties. With physical properties that are different from bulk materials, size effects on nanomaterials make them hold great promise for applications in diverse fields such as nanoelectronics, opto-electronics, and nano-biotechnology. In particular, 1D metallic nanowires draw great scientific and technologic interests due to their novel physical properties and potential applications as interconnects in future generations of nanoscale electronic devices [1].

As ideal building blocks for nanoelctronics, 1D nanostructures can function both as wiring and as device elements in architectures for nanoscale devices. Metallic nanowires can present an electrical conductance quantization [2], and show extremely low or even negative optical permittivity in a wide range, behaving similar to optical band gap (photonic crystal) materials, such as semiconducting nanowires [3].

Ordered metallic nanowires are very important for constructing scaled-up functional devices used as probes and storage devices [4]. Synthesizing nanowire arrays on an electrode makes it possible to contact the device directly as is shown in Figure 1.1 and Figure1.2. These applications have fostered great interest in fabricating copper nanowire arrays on metal electrodes.

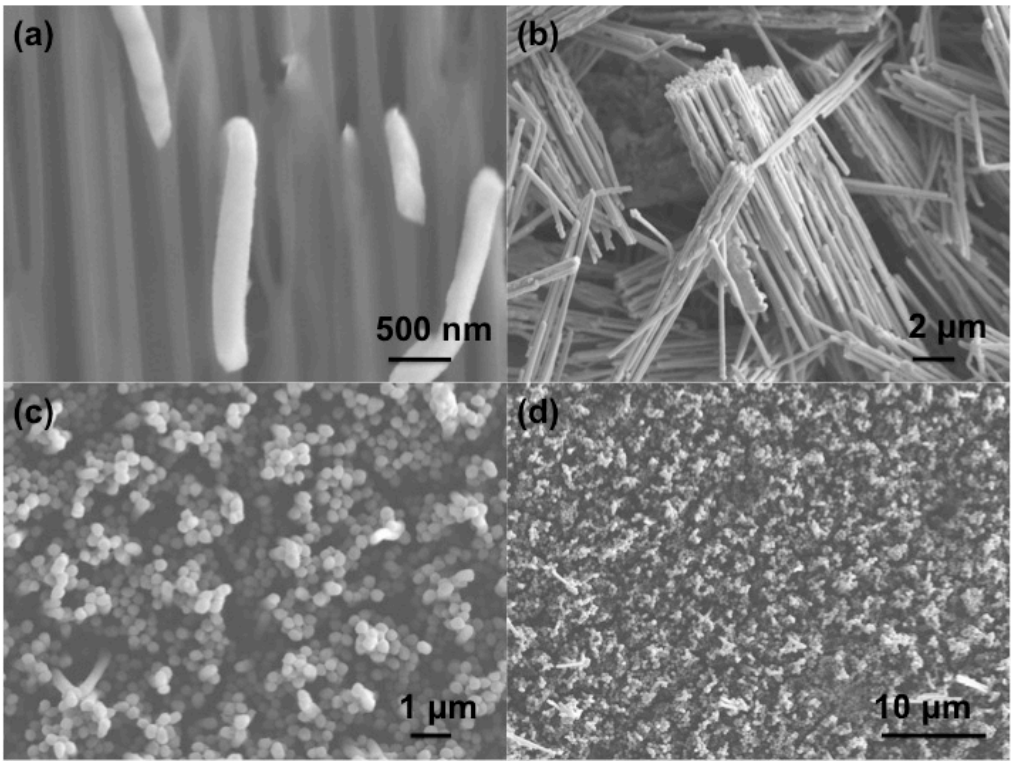

Figure 1.1. Scanning Electron Microscopy (SEM) images of various magnifications of copper nanowire arrays: (a) and (b) side view images; (c) and (d) plan view images.

1.1.1 Properties of Copper Nanowires

Copper is one of the most important metals in modern electronic technology. Among all kinds of 1D metallic nanomaterials, Copper nanowires and nanorods have presented useful physical properties, such as low electric resistivity, resistance to electromigration and low cost. These properties are are suitable in microelectronics industry and for fabrication of interconnections of nanoelectronic circuits and other devices [5] .

1.1.2 Applications of Metallic Nanowires

Metallic nanowires can be used in the areas of plasmonics, nanoelectronics, nanobiotechnology, biology, superconductivity, magnetic

sensors based on the giant magneto-resistance effect, ultrahigh-density magnetic recording media systems, high-density magnetic nanowires, low-voltage field emitter arrays, thermoelectric devices, infrared polarizers, metallo-dielectric photon crystals, and anisotropic optical filters [6]. With the rapid shrinking in size of electronic devices, metallic nanowires may play an important role in areas of nanoelectronics and optoelectronics. With the scale between 10-200 nm, metallic nanowires can connect molecular scale devices to the macroscale world, and connect elements in nanoelectronics [7].

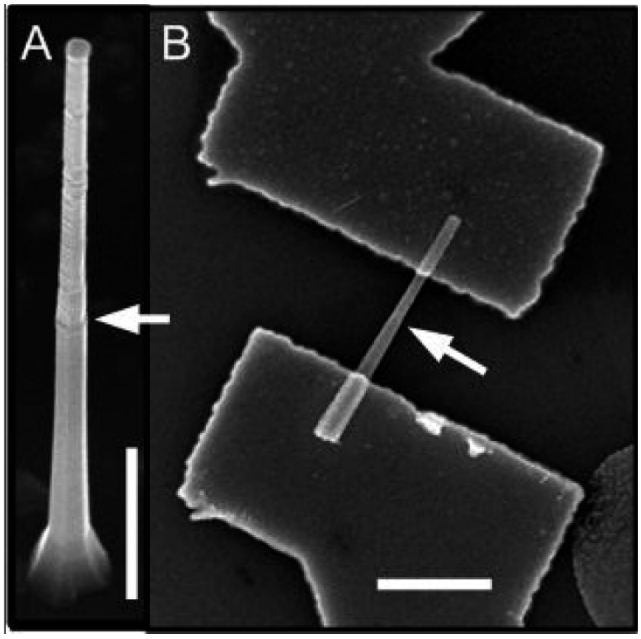

Figure 1.2. (A) SEM image of a nanowire as-grown on substrate, tilted 45°. Scale bar 0.5 μm. (B) SEM image of a tunnel diode device. Scale bar is 1 μm. In both images the InP-GaAs heterojunction is indicated by an arrow[8].

Among various 1D nanomaterials, copper draws the most interest and is one of the most commonly used materials for fabricating devices. Copper nanowires have potential applications in devices, such as wire-grid polarizers,

electrostatically dissipative devices, and current collectors for Li-ion batteries [9]. Moreover, compared with thin films, the nanowire geometry allows for radial strain relaxation, permitting a much broader range of materials combinations. Thus, nanowires could potentially be used for high-performance solar cells produced on low-cost silicon substrates [8].

1.2 Synthesis of Metallic Nanowires

There are many different methods to prepare nanowires. Basically, they can be categorized as “Top Down” and “Bottom Up” approaches, which are also classified as methods used in fabrication of nanoelectronic devices.

The top-down approach often uses the traditional workshop or microfabrication methods where externally controlled tools are used to cut, mill, and shape materials into the desired shape and order. Patterning techniques, such as photolithography and inkjet printing belong to this category. In contrast, the bottom-up approach selectively adds atoms to create structures instead of taking material away to make structures. Examples are solution based approaches such as hydrothermal and sol-gel approach, chemical vapor deposition, physical vapor deposition including sputtering coating and electron-beam evaporation.

Although much effort has been devoted to improve the synthesis techniques, most of these methods take place under severe processing conditions, can be expensive and are only applicable to a small number of material systems. Moreover, the nanowires obtained using these methods are not sufficiently long and straight for nano-scaled device applications. Other

drawbacks of these techniques include complicated implementation and the difficulty to remove the hard templates [10].

1.2.1 Electrodeposition for Synthesizing Metallic Nanowires

In recent years, electrodeposition methods based on nanoporous templates, pioneered by Possin in the 1970s [11] and C.R. Martin in the 1990s [12], have provided a versatile approach and has been widely used to prepare freestanding nanowires of metals, semiconductors, and polymers [13].

As one of the most successful approaches to fabricate nanowires, electrodeposition based on templates is a “Bottom Up” technique using a patterned electrochemical replication of the cylindrical pores of nonconductive porous membranes. This approach is widely used because of its efficiency, large scale, easy implementation, versatility, rapid-reaction, good control over stoichiometry and cost-effectiveness. It is proved that electrodeposition methods are generally inexpensive with the ability to deposite various nanowire materials and create a wide range of nanowire diameters (5 nm to 10 μm). Moreover, the aspect ratios (length to diameter ratios) of these wires can achieve as high as 1000 can be achieved with good control of the length and diameter [6].

Figure 1.3 is a schematic for the procedures of template synthesis of nanowires, including coating 30-200 nm gold layers on one surface of AAO, electrodepositing materials inside the pores of AAO, and etching of the template after nanowires to achieve a certain length. Following the schematic procedures, freestanding nanowires can be obtained as is seen in Figure 1.4. It is shown

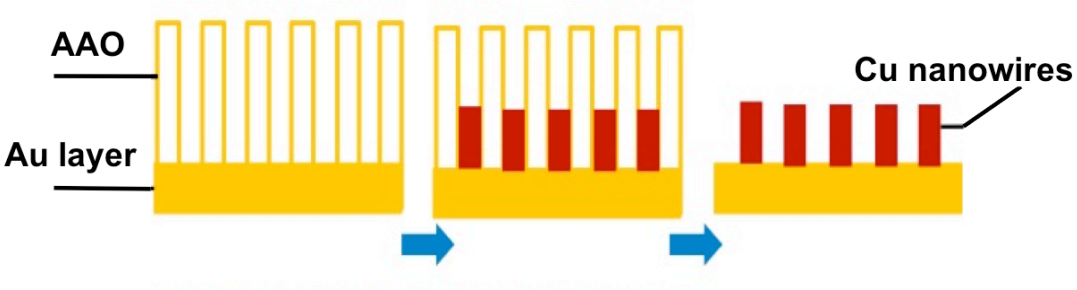

Figure 1.3. Schematic of the procedure of template synthesis of nanowires.

that even after the template is dissolved, the copper nanowires can keep standing in arrays on the gold layer as they were embedded in templates.

However, it is still difficult to control the crystallinity of nanowires grown by electrodeposition. Most of them are polycrystalline with or without a preferred growth orientation. It has been reported recently that single-crystal copper nanowires have been synthesized in both polycarbonate (PC) and anodic alumina membranes by electrodeposition method using a reverse pulse technique in ultrasonic field or conventional direct current plating at room temperature [1]. The diameters of these wires range from micrometers down to nanometers (~70 nm). However, the growth mechanism and the relationship between the electrodepositing conditions and the crystalline structures of nanowires are not entirely clear.

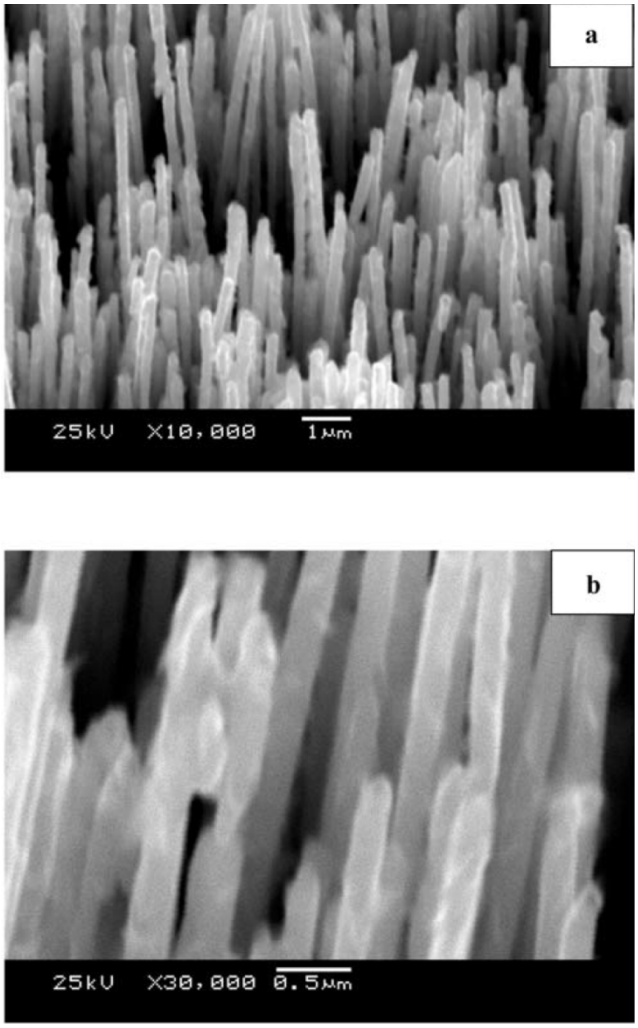

Figure 1.4. SEM micrographs of the exposed Cu nanowires after the alumina template membrane were dissolved away. (a) ×10 000. (b) ×30 000 [6].

1.2.1.1 The Influence of Experimental Parameters on Nanowires

Chen et al. studied the influence of electrolyte and electrodeposition time on the uniformity of copper nanowire lengths [14]. According to these authors, freestanding copper nanowires (aspect ratio 17–20) can be obtained in alkaline electrolyte, whilst nanowires electrodeposited in very acid electrolyte showed the worst uniformity of length. Liu et al. [15], found that both morphology

and crystalline structure of copper nanowires were influenced by the deposition potential.

Table 1.1 presents a brief overview of literature results for the texture coefficients for copper nanowire arrays, obtained by applying various conditions for synthesis. Preparation conditions including types of membranes, thickness of membranes, nominal pore size (d_N), bath (electrolyte) conditions, applied deposition potentials and mean diameter of the synthesized copper nanowire (d) are also depicted. However, it is difficult to extract the parameters that most influence crystallinities from these data.

Table 1.1. Literature reviews of texture results for copper nanowire arrays obtained by electrodeposition into different nanoporous templates as a function of the preparation conditions.

Preferred (hkl)	**Membrane**	**Bath**	**mV**	**Nanowire Diameter (nm)**
(111) [16]	AAO, 30 μm, d_N=60 nm	0.2 M $CuSO_4$, 0.1 M H_3BO_3, pH = 4.5–5.0, RT.	-232	58-62; d=60
(220) [17]	AAO, 30 μm, d_N =60nm	0.2 M $CuSO_4$, 0.1 M H_3BO_3, pH = 4.5–5.0, RT.	-532	58-62; d=60
(220) [18]	PC, 30, 40 μm, d_N=30–200 nm Typical 60 nm	0.95 M $CuSO_4$ ·5H_2O, 21 g/L H_2SO_4 pH=0	-50	30-60
Without preferred orientation [19]	AAO, 60 μm, d_N= unspecified	300 g/L $CuSO_4$, 45 g/L H_3BO_3, pH = 2.5	2.5 mA/cm^2	90
(200) [6]	AAO, 60 μm, d_N=20nm	0.5 M $CuSO_4$ ·5H_2O, pH=1,RT.	-250	150

1.2.1.2 The Importance of Additives during Electrodeposition

Generally known as a pH buffer, H_3BO_3 is a conventional additive for electrodeposition. By using H_3BO_3, a constant pH value can be achieved due to the release of protons in the cathodic diffusion layer [20]. Moreover, boric acid can change the morphology of the deposited film to improve the smoothness of depositing surface, resulted from a better crystallization performed[21]. Also, it is reported that the deposition rate is affected by the concentration of boric acid in the solution [22]. Boric acid can be adsorbed on the surface of the electrode and decrease the discharge rate of hydrogen. This increases the overpotential for hydrogen evolution and improves the deposition efficiency [22].

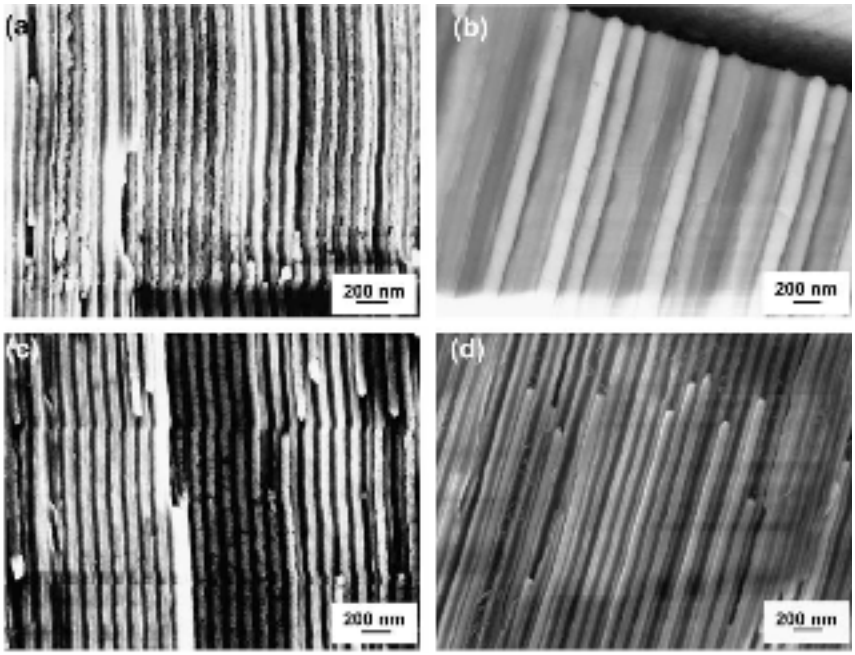

Figure 1.5. Cross-sectional high-resolution SEM micrographs of alumina template filled with Fe nanowires deposited at 1.1 V for 10 min using: (a) 0.1 M $FeSO_4$ + 0.525 M Na_2SO_4; (b) 0.1 M $FeSO_4$ + 0.525 M Na_2SO_4 + 0.4 M H_3BO_3; (c) 0.5 M $FeSO_4$+ 0.525 M Na_2SO_4; (d) 0.5 M $FeSO_4$ + 0.525 M Na_2SO_4 + 0.4 M H_3BO_3 [23].

As for the electrodeposition of synthesizing nanowires, boric acid also plays an important role in efficiently stabilizing the pH, avoiding the formation of hydroxides and enhancing the surface characteristics towards smooth, compact and continuous nanowires [23] as is shown in Figure 1.5.

1.2.2 Templates for Synthesizing Metallic Nanowires

The templates used in electrodeposition have been extensively investigated in the synthesis of different nanostructures. The most commonly used and commercially available nanoporous templates are block copolymer thin films with cylindrical nanopores, anodized aluminum oxide (AAO), and radiation track-etched polycarbonate (PC) membranes [24].

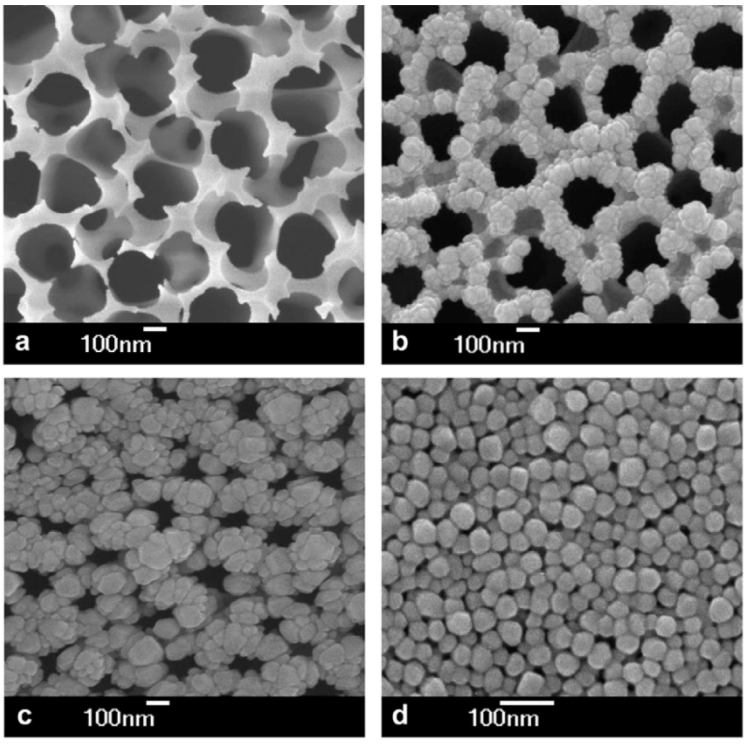

Figure 1.6. SEM images of the backside of AAO membranes with Au sputtering for: (a) 0 min, (b) 10 min, (c) 15 min, and (d) 20 min [25].

Other membranes have also been used, such as nanochannel arrays on glass, radiation track-etched mica, mesoporous materials, and porous silicon by electrochemical etching of silicon wafer, zeolites and carbon nanotubes. The commonly used alumina membranes with uniform and parallel pores are made by anodic oxidation of aluminum sheet in solutions of sulfuric, oxalic, or phosphoric acids.

The AAO pores can be arranged in a regular hexagonal array and densities as high as 10^{11} pores/cm^2 can be achieved [26]. Before nanowire synthesis, the templates are always coated with a thin layer of conductive material, e.g. gold as is shown in Figure 1.6.

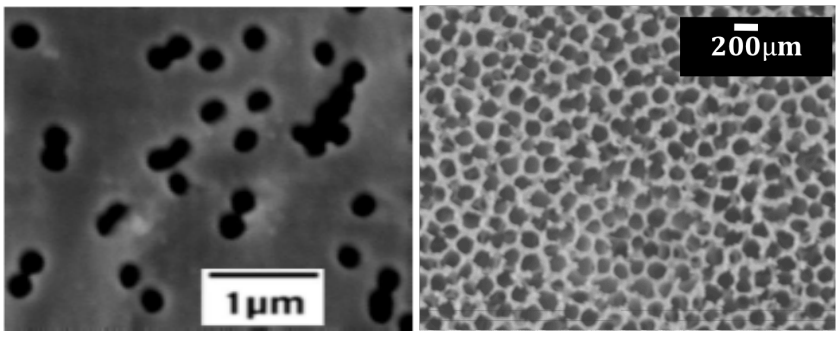

Figure 1.7. SEM images of (a) Polycarbonate membrane[27], and (b) AAO membrane.

Moreover, the alumina templates have received much attention because of their good characteristics for nanowire array fabrication. They are thermally and mechanically stable and can be produced with a high density of high-aspect-ratio, parallel, and nearly uniform pores (ranging from 10 nm to several hundred nanometers) as is presented in Figure 1.7. Furthermore, the

alumina pore diameter can be simply and inexpensively tuned from 10 nm to > 100 nm by varying the anodization conditions [24].

1.3 Single-Crystal Nanowires

The single crystalline form is used in the semiconductor device fabrication since grain boundaries would bring discontinuities and favor imperfections in the microstructure of nanomaterials, such as impurities and crystallographic defects, which can have significant effects on the local electronic properties of the material.

On the scale that devices operate, these imperfections would have a significant impact on the functionality and reliability of the devices. As to a microprocessor, without the crystalline perfection, it would be virtually impossible to build Very Large-Scale Integration (VLSI) devices in which billions of transistor-based circuits, all of which must reliably be working, are combined into a single chip.

The studies in previous literature are listed in Table 1.1. The data demonstrate that electrochemically formed copper nanowire arrays can be obtained as polycrystalline (without any texturing degree) or textured with each of the (111), (200) or (220) preferential orientation in a face center cubic (fcc) structure.

1.4 Research Preview and Goals

Considering the properties of relatively high conductivity and low cost of copper among all metal materials, studies have been done about the synthesis

and characterization of copper nanowires. Here, the electrochemical approach is chosen to grow copper nanowire arrays into the high aspect ratio channels of the AAO membranes. For cost reasons, we use AAO membranes that are primarily intended as filter elements with relatively large pores of 200 nm.

Although our AAO has been designed for filtration, it can also be used as nanostructure templates to prepare nanowires due to the pore size and thickness of the membrane. Together with electrodeposition, template synthesis is inexpensive and has high productivity of many kinds of nanowires with suitable precursors provided. However, nanowire technology is still in the initial phase and needs further investigation using template approach to synthesize single-crystal nanowires.

In this work, the influence of electrodeposition operation conditions, such as deposition potential and electrolyte concentration, on the morphology and crystallinity of copper nanowires are investigated. Copper nanowire arrays fabricated by the template method were released from the AAO templates and dispersed on silicon wafer surfaces. The morphologic information, e.g. diameter and length, of copper nanowires was characterized by SEM. The composition and texture of nanowires embedded in templates were determined by XRD. After being released from the template, single nanowires were characterized by electron diffraction recorded with a TEM. Finally, the differences between the morphology and crystallinity of nanowires synthesized by changing independent parameters were analyzed. Studies to explore other metallic nanowires are discussed. The specific goals of the research are (i) to investigate the

relationship between experimental conditions and the crystallographic orientations of copper nanowires by electrodeposition, and to find the optimized conditions to obtain single-crystal nanowires; (ii) to find the effects of deposition conditions on morphology and growth rate of copper nanowires; and (iii) to expand the results and analysis to other metallic nanowires synthesized by electrodeposition and explore the applications of single-crystal nanowires.

1.4 References

1. Tian, M. L.; Wang, J. U.; Kurtz, J.; Mallouk, T. E.; Chan, M. H. W., Electrochemical growth of single-crystal metal nanowires via a two-dimensional nucleation and growth mechanism. *Nano letters* **2003,** *3*, 919-923.

2. Garcia, N.; Ponizovskaya, E. V.; Xiao, J. Q., Zero permittivity materials: Band gaps at the visible. *Applied Physics Letters* **2002,** *80*, 1120-1122.

3. Inguanta, R.; Piazza, S.; Sunseri, C., Novel procedure for the template synthesis of metal nanostructures. *Electrochemistry Communications* **2008,** *10*, 506-509.

4. Cao, H.; Wang, L.; Qiu, Y.; Zhang, L., Synthesis and I–V properties of aligned copper nanowires. *Nanotechnology* **2006,** *17*, 1736-1739.

5. Zhou, W. F., G.; Li, X. ; Xu, S.; Chen, L; Wu, B.; Zhang, L., In Situ X-ray Diffraction Study on the Orientation-Dependent Thermal Expansion of Cu Nanowires. *J Phys Chem C* **2009,** *113*, 5.

6. Riveros, G.; Gómez, H.; Cortes, A.; Marotti, R. E.; Dalchiele, E. A., Crystallographically-oriented single-crystalline copper nanowire arrays electrochemically grown into nanoporous anodic alumina templates. *Applied Physics A* **2004,** *81*, 17-24.

7. Zhang, J.; Sun, J.; Liu, W.; Shi, S.; Sun, H.; Guo, J., Synthesis of copper nanowires under a direct current electric field. *Nanotechnology* **2005,** *16*, 2030-2.

8. Wallentin, J.; Persson, J. M.; Wagner, J. B.; Samuelson, L.; Deppert, K.; Borgstrom, M. T., High-performance single nanowire tunnel diodes. *Nano Lett* **2010,** *10*, 974-9.

9. Inguanta, R.; Piazza, S.; Sunseri, C., Influence of the electrical parameters on the fabrication of copper nanowires into anodic alumina templates. *Applied Surface Science* **2009,** *255*, 8816-8823.

10. Cho, Y.; Huh, Y., Synthesis of ultralong copper nanowires by reduction of copper-amine complexes. *Materials Letters* **2009,** *63*, 227-229.

11. Possin, G. E., A Method for Forming Very Small Diameter Wires. *Science* **1970,** *41*, 3.

12. Martin, C. R., Nanomaterials: A Membrane-Based Synthetic Approach. *Science* **1994,** *266*, 6.

13. Dresselhaus, M. S. L., Y.M.; Rabin, O.; Black, M.R.; Dressel-haus, G. , *Nanowires, In Springer Handbook of Nanotechnology*. 2007; p 1.

14. Chen, X.; Duan, H.; Zhou, Z.; Liang, J.; Gnanaraj, J., Fabrication of free-standing Cu nanorod arrays on Cu disc by template-assisted electrodeposition. *Nanotechnology* **2008,** *19*, 365306.

15. Liu, X. L. H., H.P.; Zhou, J.H.; Dang, W.J., Preparation and characterization of electrodeposited ultralong copper nanowires based on AAO template. *Rare Metal Materials and Engineering* **2007,** *36*, 4.

16. Gao, T.; Meng, G. W.; Zhang, J.; Wang, Y. W.; Liang, C. H.; Fan, J. C.; Zhang, L. D., Template synthesis of single-crystal Cu nanowire arrays by electrodeposition. *Applied Physics A Materials Science & Processing* **2001,** *73*, 251-254.

17. Gao, T.; Meng, G. W.; Wang, Y. W.; Sun, S. H.; Zhang, L., Electrochemical synthesis of copper nanowires. *J Phys-Condens Mat* **2002,** *14*, 355-363.

18. Toimil-Molares, M. E.; Brotz, J.; Buschmann, V.; Dobrev, D.; Neumann, R.; Scholz, R.; Schuchert, I. U.; Trautmann, C.; Vetter, J., Etched heavy ion tracks in polycarbonate as template for copper nanowires. *Nucl Instrum Meth B* **2001,** *185*, 192-197.

19. Pang, Y. T.; Meng, G. W.; Zhang, Y.; Fang, Q.; Zhang, L. D., Copper nanowire arrays for infrared polarizer. *Appl Phys a-Mater* **2003,** *76*, 533-536.

20. Zech, N.; Landolt, D., The influence of boric acid and sulfate ions on the hydrogen formation in Ni-Fe plating electrolytes. *Electrochimica Acta* **2000,** *45*, 3461-3471.

21. Huang, H. C. L. C. S., Roughness control of electrodeposited CIS thin film. *ECS Transactions* **2010**.

22. Zuo, Z. Z., X.; Zuo, C., On the Role of Boric Acid in the Copper-Tin Alloy Bath. *Wuhan University Journal of Natural Sciences* **1999,** *4*, 5.

23. Haehnel, V.; Fahler, S.; Schaaf, P.; Miglierini, M.; Mickel, C.; Schultz, L.; Schlorb, H., Towards smooth and pure iron nanowires grown by electrodeposition in self-organized alumina membranes. *Acta Mater* **2010,** *58*, 2330-2337.

24. Byun, J.; Lee, J. I.; Kwon, S.; Jeon, G.; Kim, J. K., Highly ordered nanoporous alumina on conducting substrates with adhesion enhanced by surface modification: universal templates for ultrahigh-density arrays of nanorods. *Adv Mater* **2010,** *22*, 2028-32.

25. Hamrakulov, B. K., I. S.; Lee, M. G.; Park, B. H., Electrodeposited Ni, Fe, Co and Cu single and multilayer nanowire arrays on anodic aluminum oxide template. *Transactions of Nonferous Metals Society in Chna* **2009,** *19*, 5.

26. Cao, G.; Liu, D., Template-based synthesis of nanorod, nanowire, and nanotube arrays. *Adv Colloid Interface Sci* **2008,** *136*, 45-64.

27. Davis, D. M. Electrodeposition of Magnetic Nanowires and Nanotubes. Louisiana State University Baton Rouge, 2005.

Chapter 2 EXPERIMENT

2.1 Preparation of Copper Nanowires

Copper nanowires with nominal diameters of 200 nm were prepared by electrodeposition using commercial AAO templates purchased from Whatman (Anodisc 13 made by Whatman), which have an average pore diameter of about 200 nm, thickness of 60 μm, porosity of about 28%, and surface pore population of the order of 10^{13} pores/m^2. The membranes used in this work are typically used for filtration, but there are several reports [1] showing that copper and other metal nanowires or nanotubes [2] can be successfully prepared using them as templates. Before each electrochemical experiment, one side of the template was coated with a thin Au layer to become an electrically conductive working electrode. The Au layer was made thick enough so that a continuous layer was present at the bottom of the nanopores.

2.1.1 Sputtering Deposition

Prior to nanowire fabrication, a thin conductive layer of around 100 nm Au was sputtered on one side of the AAO using a conventional sputter coater to make this surface electrically conductive. Samples are sputtered at room temperature, although the heat emanating from the target during sputtering can elevate the temperature in the chamber to 40-50 °C. The rate of sputter coating was experimentally determined to be about 0.03 nm/s for gold. The thickness of the gold film was detected by a quartz crystal microbalance sensor and calibrated by measuring the thickness in SEM.

2.1.2 Electrochemical Deposition

Electrodeposition was done in a conventional three-electrode electrochemical cell as shown in Figure 2.1 and Figure 2.2. A potentiostat was used to control the potential of Cu electrodeposition. A Ag/AgCl electrode with saturated KCl solution (E=0.197 V vs. Standard Hydrogen Electrode, SHE) was used as a reference electrode. All potentials referred in this work are obtained according to this electrode potential if other annotations are not added. A piece of platinum flag of 1×1 cm^2 served as a counter (auxiliary) electrode. The two-piece electrochemical cell in Figure 2.2 was more effective than the one in Figure 2.1 because the AAO with gold layer can be positioned outside the electrolyte solution to minimize copper deposition on the bottom of the gold side.

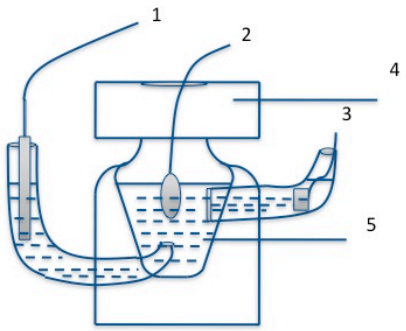

1. Reference Electrode: Ag/AgCl with Sat. KCl (E= 0.197V)
2. Working Electrode: Porous Anodic Alumina Membrane with 100 nm Au film
3. Counter Electrode: Pt flag
4. Teflon Lid
5. Electrolyte

Figure 2.1. Schematic of a three-electrode cell for preparation of copper nanowires

As shown in Figure 2.2, the pore side of the AAO membrane faces upward and the edges seal with an o-ring at the bottom of the cell. The inner

diameter of the hole and o-ring on the cell bottom determined the size of the area in contact with the electrolyte, which is 0.3 cm^2 (by geometry).

The aqueous electrolyte used was a $CuSO_4 \cdot 5H_2O$ solution with concentration of 0.1 M, 0.2 M, and 0.3 M. Boric acid (H_3BO_3) 0.1 M was added to each electrolyte. The pH was adjusted by adding dropwise diluted sulfuric acid into the electrolyte and measured by pH test paper. Electrodepositions were performed at room temperature with a potentiostat that provides a controlled applied voltage or current.

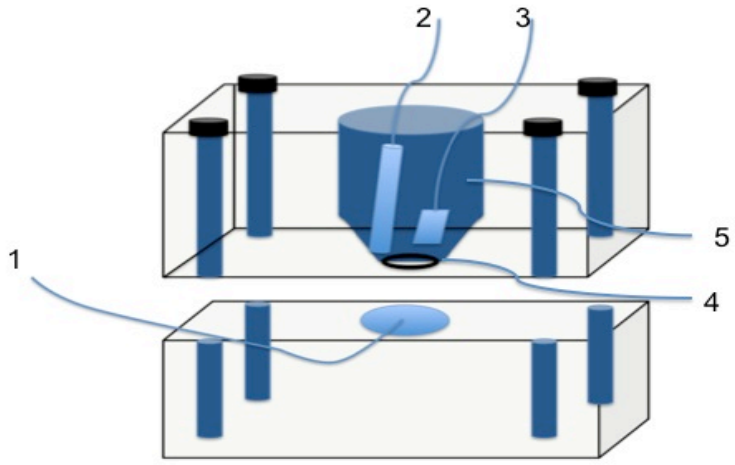

1. Working Electrode: Porous Anodic Alumina Membrane with 100 nm Au film
2. Reference Electrode: Ag/AgCl with Sat. KCl (E=0.197 V)
3. Counter Electrode: Pt flag
4. O-ring
5. Electrolyte

Figure 2.2. The three-electrode evaluation cell for electrodeposition, in which the gold side of AAO faces down to avoid touching the electrolyte inside the cell

2.1.2.1 Preparation of Working Electrode

Prior to each experiment, the gold-coated AAO membranes were soaked in electrolyte for 20 min to wet the pores with copper ions. A strip of copper tape was used to link the working electrode to the corresponding electrode of the potentiostat. Using the electrochemical cell in Figure 2.2, the AAO membrane was positioned with the pores facing up to the electrolyte and the Au side outside of the solution. However, it was observed that copper was partially deposited on the gold surface after electrodeposition. The four bolts need to be tightened at the same time to assure a uniform stress distribution onto the AAO surface to prevent the sample from being cracked during electrodeposition. Uneven tightening could partially explain the gold deposition on the backside. It was reported that nail polish could be used to produce an electrode with only one face exposed [3], but we found that the nail polish could penetrate through the pores, contaminate the gold surface and inhibit copper deposition.

2.1.2.2 Electrodeposition Techniques

In this work, it was found that different preferred orientations of copper nanowires could be fabricated by changing the electrodeposition conditions using chronoamperometry (constant potential or potentiostatic) and chronopotentiometry (constant current or galvanostatic), while varying the deposition time, the concentration of electrolyte, and the pH of the electrolyte.

Also studied were the effects of stirring the electrodeposition bath on the length distribution of released nanowires. The released nanowires dispersed

in ethanol were characterized after applying various ultrasonication durations. The effect of adding 1-Dodecanethiol to help prevent aggregation was also characterized and discussed.

2.1.2.2.1 Control-Potential Electrodeposition

During a series of electrodeposition experiments, the potential was applied as -0.2 V, -0.4 V, or -0.6 V while the other experimental conditions were held constant.

Table 2.1. Chemicals used in electrodeposition experiments

Chemicals	Description	Molecular weight/ g·mol^{-1}
Copper (Π) sulfate Pentahydrate, $CuSO_4 \cdot 5H_2O$	>=98%, crystalline	249.68
Boric acid, H_3BO_3	99+%, extra pure, power	61.83
Sulfuric acid, H_2SO_4	95.6%, 18 M, concentrated,	98.08

To prepare the electrolyte, 0.2 M $CuSO_4.5H_2O$ solution, with 0.1 M H_3BO_3 were used to prepare 0.1 L solution. Sulfuric acid was added dropwise to adjust the pH to 4.0. A sample calculation of electrolyte preparation is given below.

a. $n_{CuSO_4 \cdot 5H_2O} = \frac{m}{M}$

$$m = n \cdot M = 0.2 \times 0.1 \times 249.68 = 4.9936 g$$

b. 

$$m = n \cdot M = 0.1 \times 0.1 \times 61.83 = 0.6183 g$$

c. $n_{H_2SO_4} = 1\ M \times 10\ mL = 18\ M \times V_{H_2SO_4}$

$$V_{H_2SO_4} = 0.556\ mL$$

After adding deionized water to fill the solution container to 100 mL, 1 M aqueous sulfuric acid (a 10 ml 1 M H_2SO_4 aqueous solution was held in another container.) was added dropwise to adjust the pH to 4.0 using test paper.

The standard electrode reduction potential of the half reaction of

$$Cu^{2+} + 2e^- \rightarrow Cu \quad (1)$$

is 0.34 V (SHE) and 0.143 V (Ag/AgCl, Sat. KCl). According to Nernst equation [4] for this half reaction,

$$E_{Cu^{2+}/Cu} = E^{\theta}_{Cu^{2+}/Cu} + \left(\frac{RT}{nF}\right)\ln[Cu^{2+}_{(aq)}] \quad (2)$$

$E_{Cu^{2+}/Cu}$ represents the half-cell reduction potential at room temperature, $E^{\theta}{}_{Cu^{2+}/Cu}$ is the standard half-cell reduction potential, *R* is the ideal gas constant, *T* is the absolute temperature (in Kelvin), *n* is the number of moles of electrons transferred in the half reaction, and *F* is Faraday's constant.

In this study, *R* = 8.314 $JK^{-1}mol^{-1}$, *T*=298 K, *n*=2, *F* = 9.6485×10^4 $Cmol^{-1}$, and $E^{\theta}{}_{Cu^{2+}/Cu}$ = 0.34 V (SHE, 1 M Cu^{2+}, 1 atmosphere and 25°C). Using the example of electrolyte with 0.2 M $CuSO_4{\cdot}5H_2O$, so $[Cu^{2+}(aq)]$=0.2 M, calculation yields $E_{Cu^{2+}/Cu}$= 0.319 V (SHE) and 0.122 V (Ag/AgCl, Sat. KCl), which means when the electrodeposition potential is more negative than 0.122 V, the

reduction reaction can be performed on the working electrode (cathode). In this work, typical potentials were in the range of -0.2 to -0.6 V.

Hydrogen evolution is an electrode reaction in which hydrogen gas is produced at the cathode of an electrolytic cell by the reduction of hydrogen ions or the reduction of the water molecules of an aqueous solution. Since $E^{\theta}_{H_2O/H_2}$ = -0.83 V (SHE, 1 M hydrogen ions, 1 atmosphere and 25°C), E_{H_2O/H_2} = -0.273 V (SHE, pH=4) based on Equation (2) and -0.434 V when using Ag/AgCl reference electrode with saturated KCl aqueous solution (E=0.197 V, SHE). Considering the concurrent cathode reaction of hydrogen evolution (*E* = -0.434 V at pH=4), copper deposition could be carried out under three different situations: absence of hydrogen evolution (-0.2 V), slow hydrogen gas formation (-0.4 V), and vigorous H_2 bubble evolution (-0.6 V). In this work, three potentials in the range of -0.2 to -0.6 V were chosen to cover these three conditions [5]. H_2 bubbles were observed on the working electrode during electrodeposition when -0.4 V and -0.6 V were applied.

Also, from previous experience, copper nanowires can be more easily grown and more uniformly synthesized when choosing electrodeposition potential in the range of 0 V to -1.0 V rather than using other potentials under chronoamperometry.

2.1.2.2.2 Control-Current Electrodeposition

As an alternate to potential control, the electrodeposition current was controlled constant during a separate series of experiments. Deposition currents

of -0.7 mA, -1.5 mA, and -3.0 mA were investigated to access a region of lower current conditions than for constant potential deposition.

To prepare the electrolyte, 0.3 M $CuSO_4 \cdot 5H_2O$ solution and 0.1 M boric acid were used, with sulfuric acid added to adjust the pH around 4.0. The current was set at -0.7 mA, -1.5 mA, and -3.0 mA for 1.5 hr at room temperature.

Under constant potential conditions of -0.05 V and -0.1 V, current response is in the range of -3.5 mA to -5 mA. Therefore, considering that smaller constant current may cause different growth mechanisms of the copper nanowires, lower deposition currents were used under current control. Nevertheless, the results might not be very satisfying from the experiences when applying small deposition currents. In some cases, there were barely nanowires grown in the pores, even after long times. There may be leakage currents in our experiments so that the actual deposition current is lower than expected. This is discussed later in Section 3.2.2.

2.2 SEM, XRD and TEM Characterization

SEM measurements were performed to verify that Cu was successfully electrodeposited into the pores of AAO templates in the form of nanowires. Morphology, such as smoothness, and lengths of nanowires, either before or after the templates were dissolved can be determined from the SEM images. By measuring the length of copper nanowires inside the templates, the growth rate based on electrodeposition can be calculated and compared under different experimental conditions.

After experiments, the template embedded with Cu nanowires was immediately rinsed with deionized water and ethanol three times. They were then completely dried in air before characterization. SEM characterization of both plan views and cross-section views of copper nanowires were performed to analyze the morphology and growth rate, and correlate it with deposition potential, electrolyte concentration, and deposition time.

XRD measurements were used to investigate the phase structure and crystal orientation of Cu nanowire arrays inside AAO templates. Theta/ two-theta scans were performed for different samples. XRD analysis was performed within 12 hr after the completion of the electrodeposition to characterize the crystalline orientation of the copper nanowire arrays. The AAO templates with copper nanowires inside the pores were analyzed directly by XRD. The phase structures and crystal orientation of Cu nanowires were characterized by an X-ray diffractometer with Cu Kα1 radiation (λ = 0.154056 nm). By comparing the diffraction peaks with the standard JCPDS card of polycrystalline copper, the preferred orientation of the nanowires grown inside the channels was determined.

Transmission electron microscopy (TEM) provides more detailed analysis of the crystalline orientation of individual copper nanowires. Bright Field TEM was used to characterize individual Cu nanowires after nanowire arrays were completely released from AAO templates. The crystalline structure of single Cu nanowires was investigated by Select Area Electron Diffraction (SAED) experiments, the results of which were compared to XRD analysis. With higher

magnification and contrast, TEM provides enhanced images of single nanowires compared with SEM. We obtain more precise measures of diameter and length of freestanding or randomly selected nanowires. In particular, the growth direction can be determined by the SAED pattern.

Energy-dispersive X-ray Spectroscopy (EDS or EDX), used for elemental analysis, is applied in this work to determine the composition of the as-prepared Cu nanowires embedded in or released from the AAO templates. EDS can be performed together with SEM or TEM. Together with TEM is better because specific areas, e.g. individual copper nanowires, can be selected and characterized. (The data is not shown in this thesis.) In that case, other metallic grids, such as gold with a thin film of carbon, should be chosen rather than copper grids for holding the sample copper nanowires.

2.2.1 Cross-Section SEM Sample Preparation

Cross-sections of copper nanowire arrays embedded in AAO templates were characterized by SEM. Prior to SEM characterization, the samples were coated with a thin layer of 20-30 nm Au-Pd alloy to avoid charging during SEM observation. Charges can be easily generated when samples are not electrically conductive, which could significantly affect the quality of images, as Figure 2.3 shows.

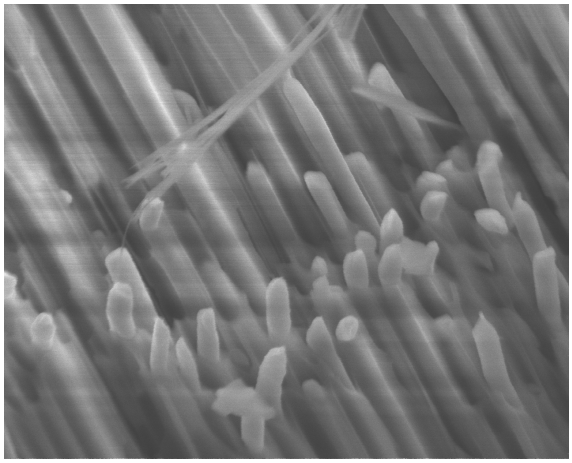

Figure 2.3. Charge effect of the copper nanowires embedded in AAO templates without Au-Pd coating before taking the SEM image

2.2.2 Template Dissolution

To completely release the copper nanowires from the AAO, 1 M NaOH aqueous solution was used to dissolve alumina at 30°C for 12 hr. The NaOH solution was then carefully replaced with deionized water by syringe extraction three times. The solid settled at the bottom during the process so that only the solution was removed. Afterwards, 1 ml ethanol and 0.1 M 1-Dodecanethiol was added to keep the nanowires spread uniformly inside the ethanol without aggregation. After the solution was ultrasonicated for 5 min, a drop of solution was dripped onto the surface of a piece of 1×1 cm^2 Si/SiO_2 wafer and dried in air. For TEM observation, a gold grid with carbon film was chosen to hold the drop of sample solution.

Pictures of released copper nanowires were taken both by SEM and TEM for characterizing the morphology and crystalline textures of single

nanowires. Using the SAED pattern, the crystallinity can be easily observed and compared with the data from XRD patterns.

2.3 Parameters of Characterization Tools

To make the AAO templates electrically conductive for acting as the working electrode, a gold layer of 100 nm was deposited on one surface of the AAO templates using a sputter coater (FTM-2000, Torr International, Inc.) in Direct Current (DC) mode. Before deposition, the chamber was pumped down to less than 5×10^{-5} torr. Using Direct Current mode, the voltage was set at 329 V and the current was 49 mA. During the deposition, argon was used as purge gas with flow rate set to 20 sccm. The sputtering was carried out in a vacuum environment of 8.55×10^{-3} torr.

Electrodepositions were carried out using a Potentiostat (VMP3, Multichannel Workstation), combined with software (EC-Lab) for recording the experimental data.

A Field Emission Scanning Electron Microscope (FESEM, JEOL JSM-6335F) was employed to take the SEM pictures of the as-prepared samples of copper nanowires before and after the AAO templates were dissolved. An environmental Scanning Electron Microscope (ESEM, Philips FEI ESEM 2020) was used for taking the picture for the AAO template itself.

The elemental analyses of samples were completed by an Energy-dispersive X-ray spectrometer (EDS, Thermo Noran System Six EDS) together with SEM morphologic observations.

The crystal orientation of the Cu nanowire arrays was analyzed by an X-ray Diffraction (XRD, Bruker D8 Advance X-Ray Diffractometer) using a θ/2θ scan with the scanning rate of 6°/min, and the 2 theta range of 40°-100°.

A Transmission Electron Microscope (TEM, JEOL 2010 FasTEM) was used for investigation of the crystallinity (Selected Area electron Diffraction) and morphology of copper nanowires (Bright Field TEM) released from templates.

2.4 References

1. Inguanta, R.; Piazza, S.; Sunseri, C., Novel procedure for the template synthesis of metal nanostructures. *Electrochemistry Communications* **2008,** *10*, 506-509.

2. Fu, J.; Cherevko, S.; Chung, C., Electroplating of metal nanotubes and nanowires in a high aspect-ratio nanotemplate. *Electrochemistry Communications* **2008,** *10*, 514-518.

3. Gerein, N. J. H., J. A. , Effect of ac Electrodeposition Conditions on the Growth of High Aspect Ratio Copper Nanowires in Porous Aluminum Oxide Templates. *Journal of Physical Chemistry B* **2005,** *109*, 14.

4. Bard, A. J. F., L. R., *Electrochemical Methods: Fundamentals and Applications*

. John Wiley & Sons, Inc.: New York, 2001; p 833.

5. Riveros, G.; Gómez, H.; Cortes, A.; Marotti, R. E.; Dalchiele, E. A., Crystallographically-oriented single-crystalline copper nanowire arrays electrochemically grown into nanoporous anodic alumina templates. *Applied Physics A* **2004,** *81*, 17-24.

Chapter 3 RESULTS AND DISCUSSION

The main objectives of this work are to investigate the effects of experimental conditions on the morphology and crystalline orientation of nanowires synthesized by electrodeposition. The growth rate of copper nanowires was measured by SEM as a function of deposition time and the experimental data was compared with calculated lengths based on Faraday's law. The relationships between the lengths of nanowires and the concentration of $CuSO_4 \cdot 5H_2O$ as well as the applied potential were also characterized and discussed. The crystalline orientations of nanowires were investigated using both potentiostatic and galvanostatic conditions, and characterized by XRD and TEM. Preferential orientations are discussed based on the Harris formula.

Potentials were chosen in a range that included 1) no hydrogen evolution (-0.2 V), 2) slow hydrogen gas formation, (-0.4 V), and 3) vigorous hydrogen evolution (-0.6 V) to examine the influence of hydrogen bubbles on the morphology and crystallinity of nanowires. Solution pH values were adjusted in the range of 4.0 to 1.0. The pH affects the conductivity of the bath and H ion adsorption, which can stabalize the growth of high-energy crystalline planes. In addition to potentiostatic experiment, galvanostatic experiments were also investigated. Galvanostatic experiments were performed to examine the effects of electrodeposition within a smaller current range (-0.7 mA, -1.5 mA, and -3.0 mA) on the crystallographic properties of nanowires.

3.1 Growth Rate of Electrodeposition

To measure the growth rate of nanowires prepared by electrodeposition at constant currents of -0.7 mA, -1.5 mA, and -3.0 mA, electrolytes were prepared with 0.3 M $CuSO_4 \cdot 5H_2O$, 0.1 M H_3BO_3, and pH adjusted to 4. All three electrodepositions were conducted for 3 hr at room temperature in the same apparatus.

Figure 3.1 presents a comparison of cross-sectional SEM images showing the lengths of nanowires embedded in AAO templates. As marked in each SEM image, the lengths of nanowires are positively correlated with the deposition current.

Nanowire lengths were also calculated according to the expression used to calculate the thickness of electrodeposits (here it is the length of nanowires) [1],

$$h = \frac{tZI}{ad} \tag{1}$$

where *a* is the surface area of AAO exposed to the electrolyte with nanopore area of 28%, *t* is the deposition time, *I* is the deposition current, *d* is the density of copper and

$$Z = \frac{M}{nF} = \frac{63.55}{2 \times 96485} = 3.293 \times 10^{-4}\, g \cdot C^{-1} \tag{2}$$

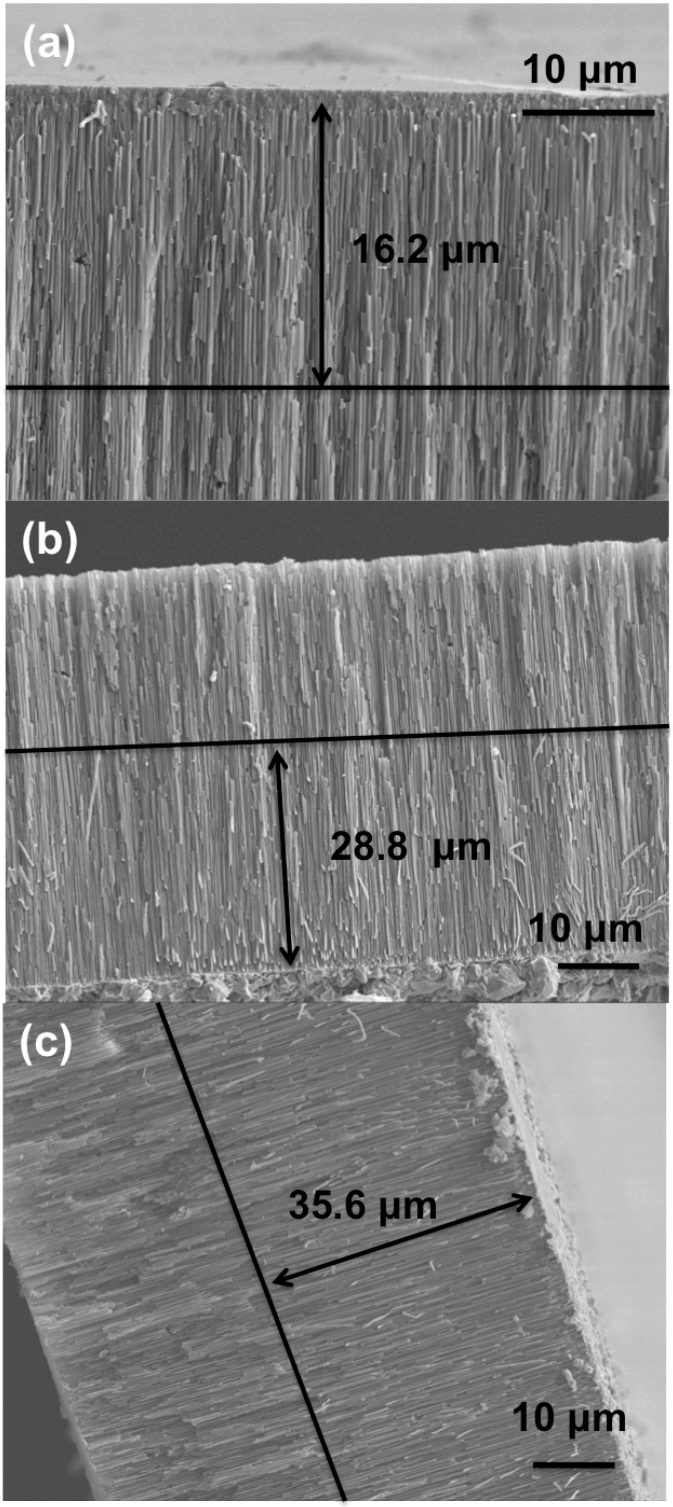

Figure 3.1. SEM images of copper nanowires grown at different deposition currents: (a) -0.7 mA; (b) -1.5 mA; (c) -3.0 mA for 3 hr. The electrolytes contain 0.3 M $CuSO_4 \cdot 5H_2O$, 0.1 M H_3BO_3, pH was adjusted to 4.

where *M* is the molecular weight of copper, *n* is the number of moles of electrons transferred, and *F* is Faraday constant. The later is also known as the electrochemical equivalent and is the mass of copper transported by 1 coulomb of electricity.

A sample calculation is included for the electrodeposition during which '-0.7 mA' was applied: $t = 3\ hr$, $d_{Cu} = 8.94\ g/cm^3$, $a = 0.2\ cm^2 \times 28\% = 0.056\ cm^2$. The thickness is calculated as $h = 49.68\ \mu m$. Following the sample calculation according to Equation (1), the calculated lengths of nanowires for constant current experiments are listed in Table 3.1 and Figure 3.2.

Table 3.1. Comparison of lengths of copper nanowires prepared at different deposition currents.

Electrodeposition Current/ mA	-0.7	-1.5	-3.0
Lengths of Copper Nanowires/ μm (by SEM)	16.2	28.8	35.6
Lengths of Nanowires/ μm (by calculation)	49.7	106.5	212.9
Growth Rate/ $nm \cdot s^{-1}$ (by SEM)	1.5	2.7	3.3

There are two possibilities to explain the difference between the SEM measurements and calculations. First, although the gold end of AAO faces down towards the lower part of the cell as shown in Figure 2.2, the electrolyte could still penetrate through the pores from the upper surface surrounded by the O-ring to the gold surface. Therefore, copper was deposited partially on the bottom of the

gold surface as well as grown inside of the nanopores. In this case, the surface area for electrodeposition and measured current is larger than the front surface area, which results in the over-estimate. Second, the high aspect ratio (the ratio of the longer dimension to the shorter dimension of a nanowire) and incomplete wettability of the AAO template makes it difficult for copper ions in the electrolyte to diffuse into pores, as pointed out by Y. Konishi et al.[2]. Slow transport exacerbates leakage currents that affect the thickness calculations.

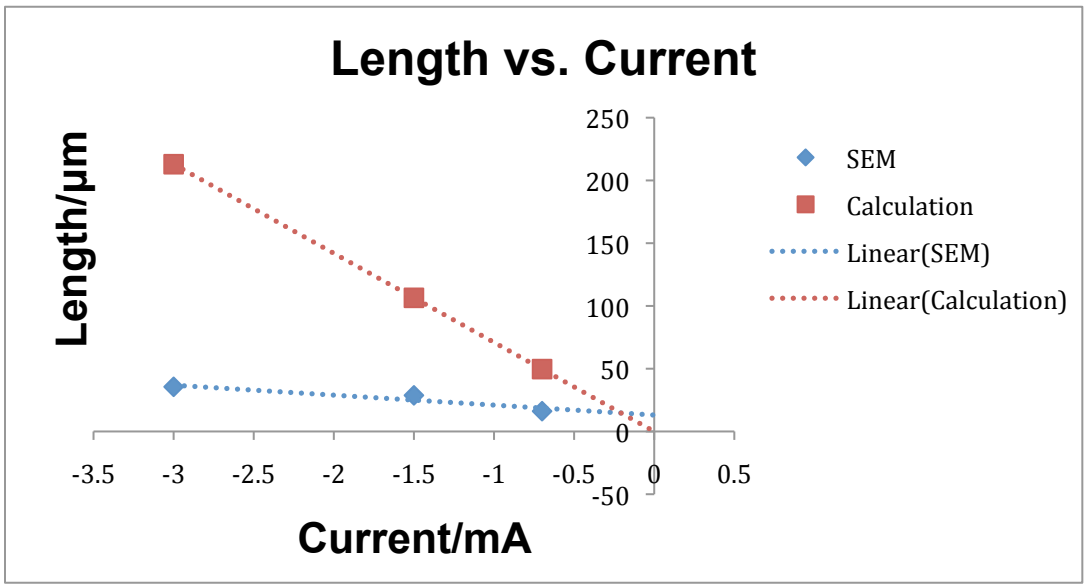

Figure 3.2. The relationship between the lengths of nanowires and electrodeposition currents. The lines are drawn as guides to the eye.

3.1.1 Electrodeposition Time and Length of Copper Nanowires

To further investigate the growth rate of copper nanowires inside templates, a group of experiments were done with three different deposition times. Copper nanowires were grown using the same conditions with 0.2 M

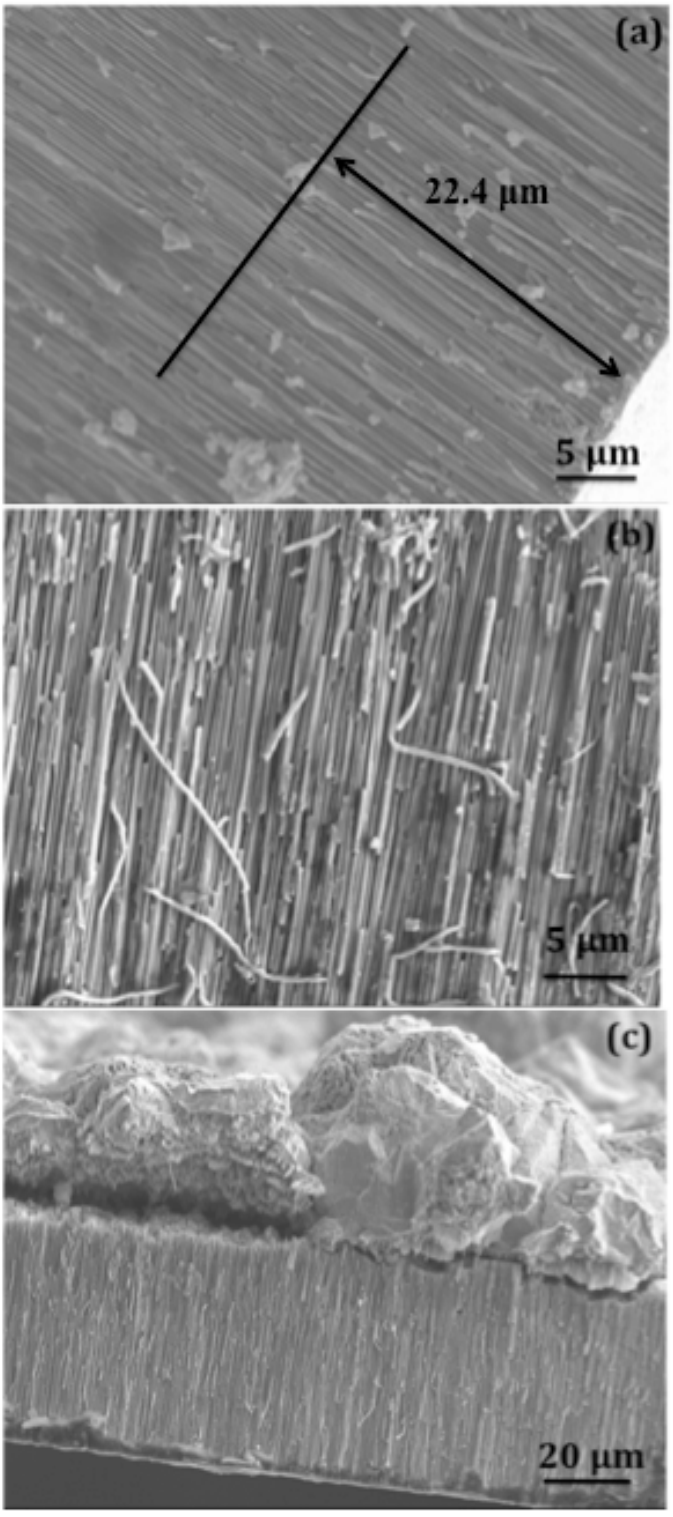

Figure 3.3. SEM images of lengths of copper nanowires grown within various electrodeposition durations: (a) 1.5 hr; (b) and (c) 3 hr. The experiments were carried out at -0.4 V in electrolytes with 0.2 M $CuSO_4 \cdot 5H_2O$ and 0.1 M H_3BO_3, pH=4.

$CuSO_4 \cdot 5H_2O$, 0.1 M H_3BO_3, pH=4 adjusted by adding dilute sulfuric acid, and constant potential of -0.4 V for 1.5 hr, 3 hr, and 5 hr.

Figure 3.3 shows the lengths of copper nanowires embedded in the templates after electrodeposition. It is clearly presented that the longer the deposition time, the longer the nanowires. In Figure 3.3 (c), copper nanowires were prepared in the same electrical conditions but with deposition time of 3 hr. It can be seen that copper has grown over the top surface of the AAO template already after 3 hr and formed a thick layer of bulk copper around 20-30 μm. Similar results were observed with 5 hr deposition time. Cap layers are formed on the template top surface once the overgrowth of nanowires occurs [3], and can grow to macroscopics sizes [4]. The lengths of nanowires for different deposition times are displayed in Table 3.2 and Figure 3.4. The final results are the mean length calculated using ImageJ (National Institutes of Health) by measuring the length of more than 20 nanowires according to the set length scale bar in each SEM image. The growth rate under these experimental conditions is 4.2 nm/sec, which is calculated based on the first experiment with deposition duration of 1.5 hr, in which copper nanowires were grown half way inside the template.

Table 3.2. Comparison between copper nanowires prepared using different electrodeposition time. * Thickness of the AAO template

Electrodeposition Time/hr	1.5	3	5
Lengths of Copper Nanowires/μm	22.4	> 60*	> 60*

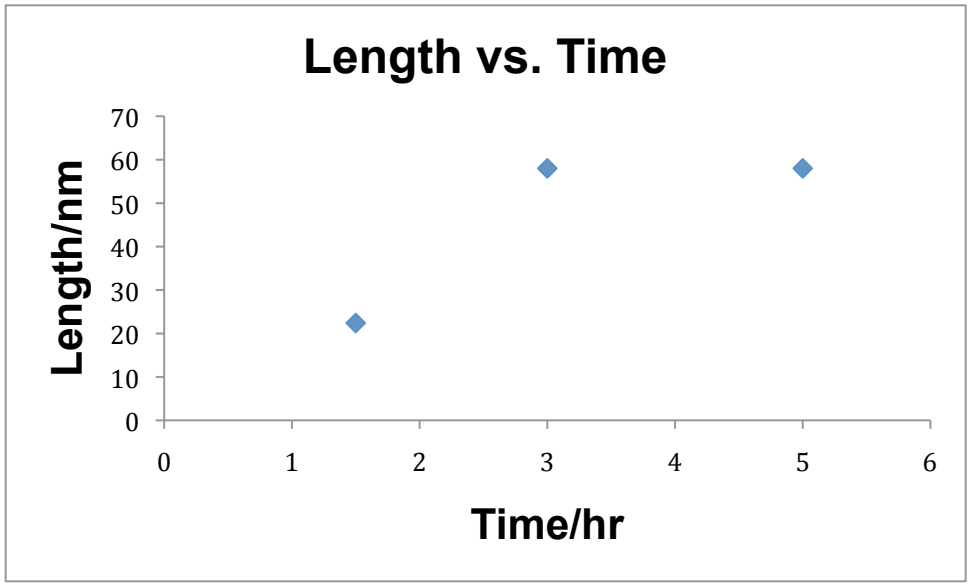

Figure 3.4. The relationship between the lengths of nanowires and deposition time.

3.1.2 Effects of Electrolyte on Growth Rate

Electrodepositions were conducted while maintaining the same depsition time of 1.5 hr, potential of -0.2 V, and pH=4, with different concentrations of $CuSO_4 \cdot 5H_2O$ of 0.1 M, 0.2 M, and 0.3 M. Cross-section SEM images of AAO templates with nanowires are shown in Figure 3.5. Data describing lengths of copper nanowires are shown in Table 3.3 and Figure 3.6. As expected, Figure 3.6 shows that the longest nanowires are synthesized when the most concentrated electrolyte with 0.3 M $CuSO_4 \cdot 5H_2O$ was employed. The growth rate of copper nanowires appears linearly related with the concentration of $CuSO_4 \cdot 5H_2O$ since other variables were all maintained constantly in this experiment. However, according to Tafel equation [5], Nernst equation [5] and Equation (1) in Section 3.1, the length of nanowires should be exponentially related with the concentration and the applied potential. It is known that when

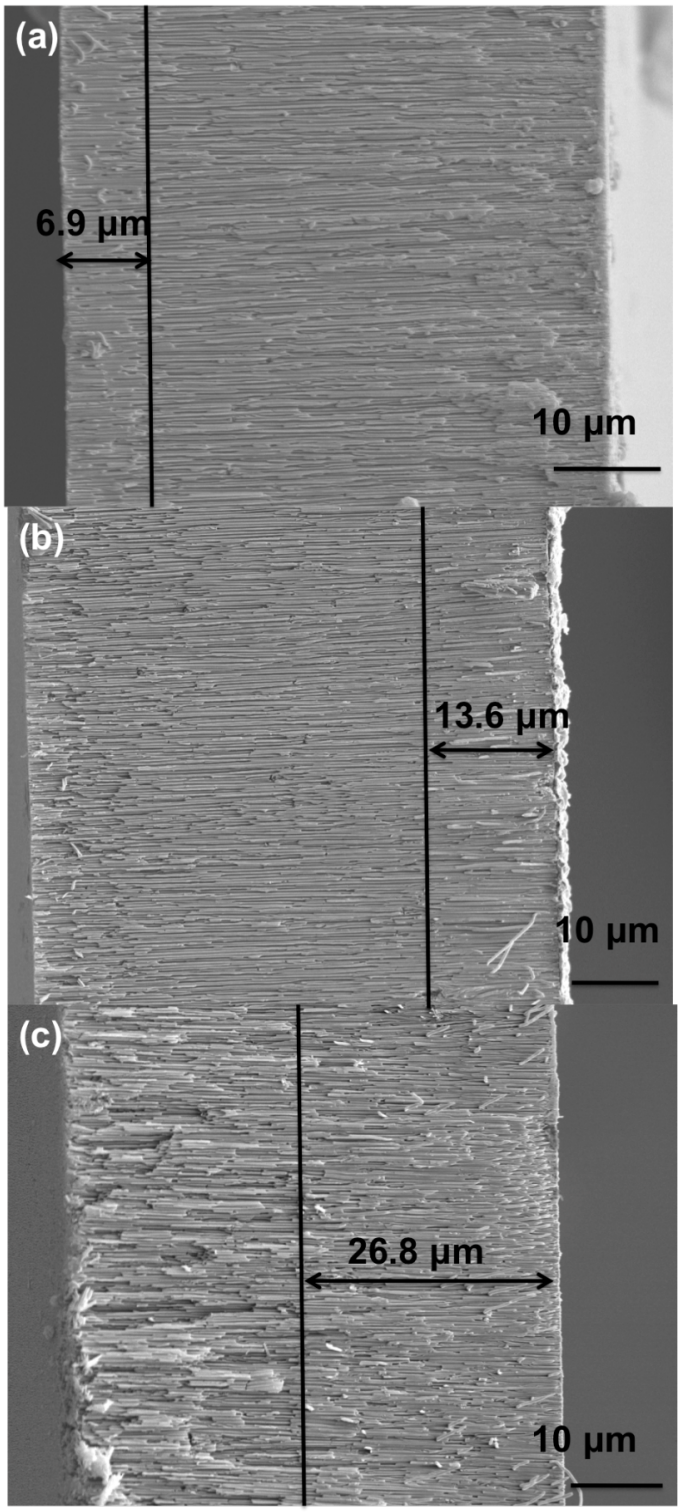

Figure 3.5. SEM images of copper nanowires prepared in electrolytes with various concentrations of $CuSO_4 \cdot 5H_2O$. (a) 0.1 M; (b) 0.2 M; (c) 0.3 M and 0.1 M H_3BO_3 at -0.2 V for 1.5 hr, pH=4.

more copper ions reach into the pores by diffusion, the amount of deposited copper will also be increased. Furthermore, when a higher concentration is employed, the reduction potential calculated using Equation (2) in Section 2.1.2.2.1 is higher than for the lower concentration. This change of reduction potential leads to a larger effective overpotential and faster growth of nanowires.

Table 3.3. Comparison between lengths of copper nanowires when the concentrations of $CuSO_4 \cdot 5H_2O$ in electrolytes were different. Deposition time: 1.5 hr.

Electrolytes /M	0.1	0.2	0.3
Lengths of Copper Nanowires /μm	6.9	13.6	26.8

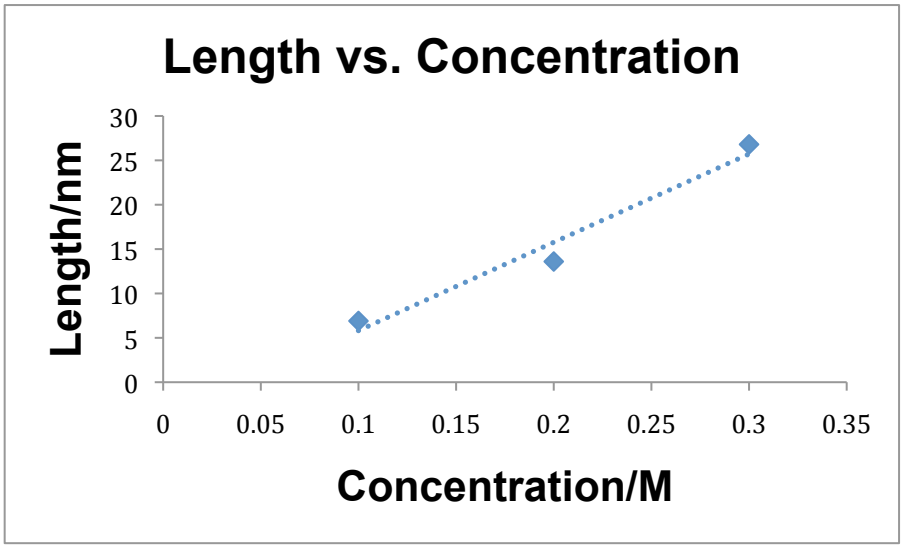

Figure 3.6. The relationship between the length of nanowires and concentration of $CuSO_4 \cdot 5H_2O$ in electrolytes. The fit is drawn as a guide to the eye.

For example, $E_{Cu^{2+}/Cu}$ is equal to 0.355 V (SHE) when $\left[Cu^{2+}(aq)\right]$=0.3 M, which is higher than 0.319 V (SHE) for 0.2 M $CuSO_4 \cdot 5H_2O$. Since the

electrodeposition potential needs to be more negative than the reduction potential to make the reaction occur, reaction with a more positive reduction potential is easier to be carried out with less negative potential applied. These data are consistent with previous reports that a high concentration of $CuSO_4 \cdot 5H_2O$ can accelerate growth of nanowires [6].

3.1.3 Effects of Potential on Growth Rate

To study the influence of deposition potential on the growth rate of nanowires, experiments were carried out with deposition potentials of -0.2 V, -0.4 V, and -0.6 V. Electrolytes were prepared with the same procedures, containing 0.2 M $CuSO_4 \cdot 5H_2O$, 0.1 M H_3BO_3, and pH adjusted to 4. All three electrodepositions were conducted for 1.5 hr at room temperature.

Figure 3.7 with SEM images of cross-sections of AAO shows the lengths of copper nanowires grown under the above conditions. Results of the lengths of nanowires are summarized in Table 3.4 and Figure 3.8. From Figure 3.7, the lengths of nanowires are positively correlated to the absolute value of the potential applied during electrodeposition. Since the current density is determined by the applied potential, the larger the potential, the larger the current density. The thickness of deposited material (here it is the length of copper nanowires) has direct relation with the current density as explained in Equation (1) of Section 3.1. According to Gao et al.'s work [7] and previous reports [8], the higher the overpotential, the higher the nucleation rates and the larger the nucleation sites in the electrodeposition process. However, nanowires with

polycrystalline character may be obtained at a high overpotential, which will be discussed later.

The potential dependence of nanowire growth rate was also investigated by observing the complete pore filling of the template for different deposition periods and potentials. As expected, nanowires reached the surface of an AAO template fastest when applying the most negative potential, but the growth rate is nonuniform, resulting in partial filling of the pores under constant potential electrodepositions. Unipolar pulsed potential depositions[9] have been used by others to synthesize copper nanowires and have demonstrated good control over the length uniformity of nanowire arrays at more negative potentials. However, the growth rate was smaller in comparison to constant potential, and further decreased with the total deposition time[9].

Table 3.4. Comparison of lengths between copper nanowires prepared at different deposition potentials. Deposition time: 1.5 hr.

Electrodeposition Potential/V	-0.2	-0.4	-0.6
Lengths of Copper Nanowires/μm	23.7	27.8	37.7

As displayed in Figure 3.7, the lengths of nanowires synthesized at -0.2 V and -0.4 V in Figure 3.7 (a) and (b), respectively, are much less uniform than ones in Figure 3.7 (c) that are obtained at -0.6 V. Although higher deposition potentials contribute to faster growth initially, hydrogen gas evolution is also enhanced at more negative potentials and the bubbles generated may accumulate and block pores to retard the deposition rate [9]. Thereby, more

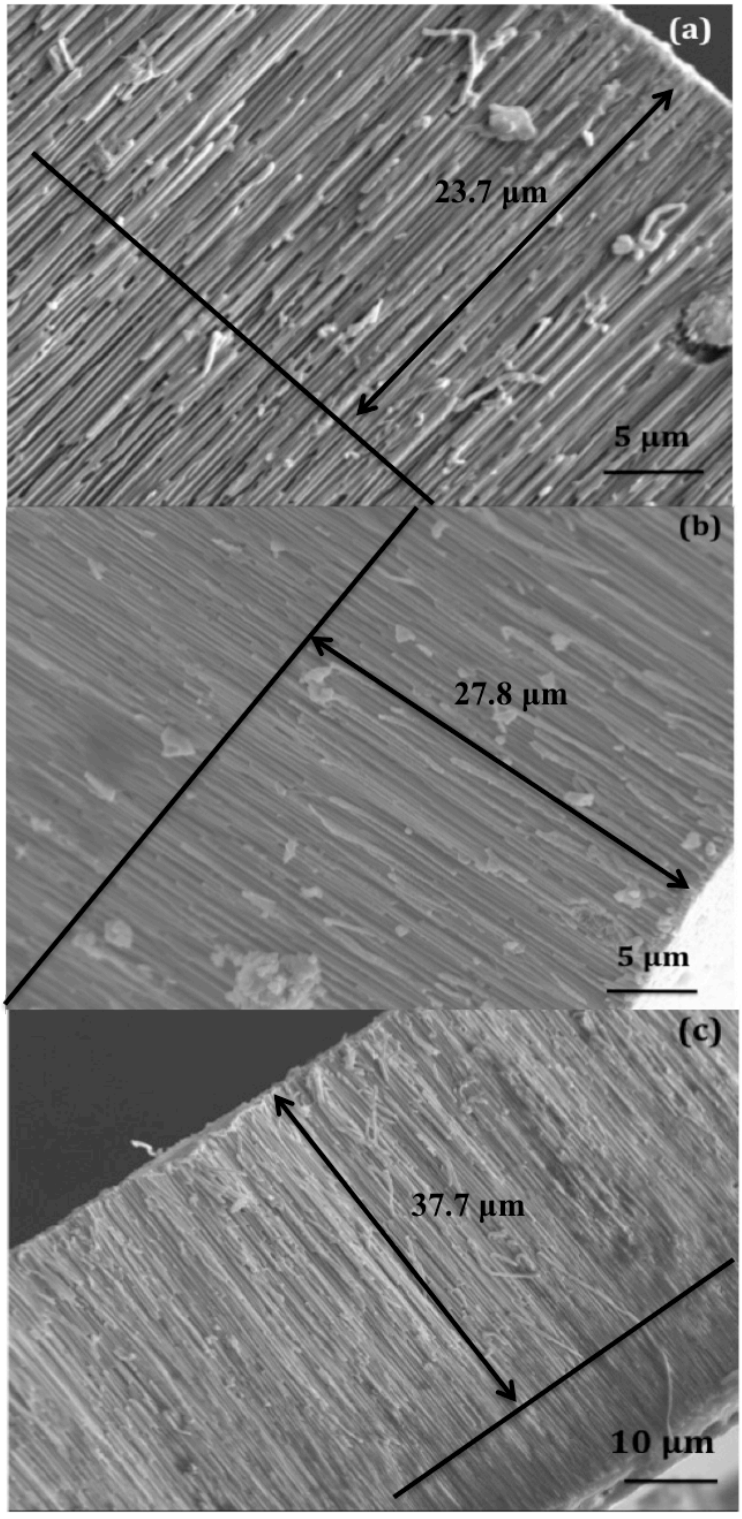

Figure 3.7. SEM images of copper nanowires grown at different deposition potentials: (a) -0.2 V; (b) -0.4 V; (c) -0.6 V for 1.5 hr. The electrolytes contain 0.2 M $CuSO_4 \cdot 5H_2O$ and 0.1 M H_3BO_3 with pH=4.

uniform growth can be achieved due to the feed back effect. Also, the enhanced uniformity could be caused by a progressive depletion of Cu^{2+} ions within membrane channels (mass transport). The copper ion consumption is faster than transport toward the electrode surface at this potential and reduces non-uniformity due to reaction conditions [4, 10, 11].

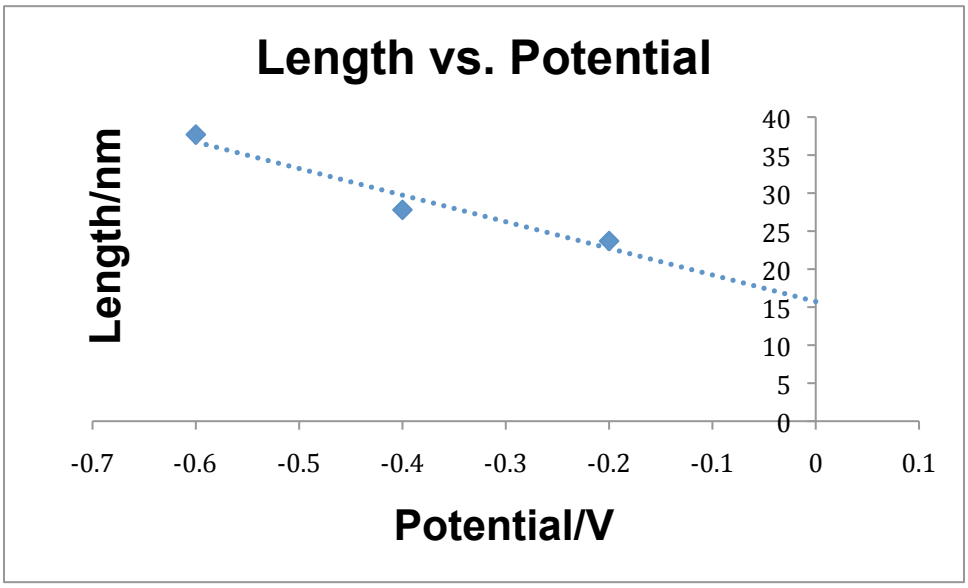

Figure 3.8. The relationship between the lengths of nanowires and the electrodeposition potentials. The lines are drawn as guides to the eye.

In summary, we observe a positively correlated dependence of nanowire growth rate on deposition current (galvanostatic conditions), electrolyte concentration, and overpotential. The observed growth rates are qualitatively consistent with calculations based on charge, but the magnitudes are different due to errors in the deposition area and possible leakage currents of unknown origin. At high potential, we observe a feedback effect due to hydrogen bubbles that retard growth. Mass transport limitations may also improve non-uniformity at

higher potentials. However, as discussed below, high potentials may impede efforts to control the crystallinity of the nanowires, so further work needs to be done to improve growth rate uniformity at lower potentials.

3.2 Crystalline Structure of Copper Nanowires

It is well known that structural and geometrical factors can play an important role in determining the various attributes, e.g., the electrical, optical and magnetic properties of nanowires [7, 11-13]. Tian et al.[14] have proved that single crystalline Au, Ag, and Cu nanowires can be prepared with a preferred (111) orientation using electrodeposition in the pores of track-etched polycarbonate membranes. In G. Riveros' work [10], highly crystallographically-oriented single-crystal copper nanowires with a (100) growth facet were electrochemically deposited into nanoporous alumina templates. Also, it was reported that copper and gold nanowires grown along the (220) plane were obtained in a potentiostatic direct current (dc) electrodeposition, whereas (200) orientation was observed under alternating current (ac) deposition conditions[15].

In spite of the numerous studies on the electrochemical deposition of metal nanowires, the literature data on the effects of electrodeposition conditions on the textures of nanowires are contradictory. To expand on the results from those studies, here we select several control variables to investigate the influence of growth parameters on the crystallographic character of copper nanowires during electrodeposition. The variables include the deposition potential using a potentiostatic technique, electrolyte composition, solution pH, and the deposition current using a galvanostatic technique. Parameters that may

also be important, but that weren't extensively studied here, include the AAO template properties (pore diameter and length), electrolyte type, Au thin film thickness on the backside of the AAO membranes, solution temperature, and the reactor configuration. Pore size and electrolyte type are briefly considered in Chapter 4.

3.2.1 Crystallinity of Copper Nanowires at Constant Potential

It has been reported that lower overpotentials are necessary to obtain single-crystal metallic nanowires by potentiostatic electrodeposition [16]. The belief is that high overpotential will cause high nucleation rates, large nuclei, and hydrogen evolution, resulting in polycrystalline copper nanowires. Consistent with these ideas, Molares et al. [11] decreased current density, which is equivalent to increased electrodeposition temperature, and observed the deposition of large crystals with the goal to fabricate single-crystal copper nanowires. Gao et al.[7] observed that as the applied potentials become more negative, nanowires began to show two sets of diffraction spots in SAED, indicating polycrystalline structures. In this work, the potentiostatic electrodeposition of the copper nanowires was performed at room temperature in electrolyte containing a mixture of 0.2 M $CuSO_4 \cdot 5H_2O$ and 0.1 M H_3BO_3 aqueous solutions. The pH of the solution was controlled around 4.0 by adding 0.1 M H_2SO_4 solution. The electrodeposition was carried out at three different deposition potentials of -0.2 V, -0.4 V, and -0.6 V, each for 1.5 hr.

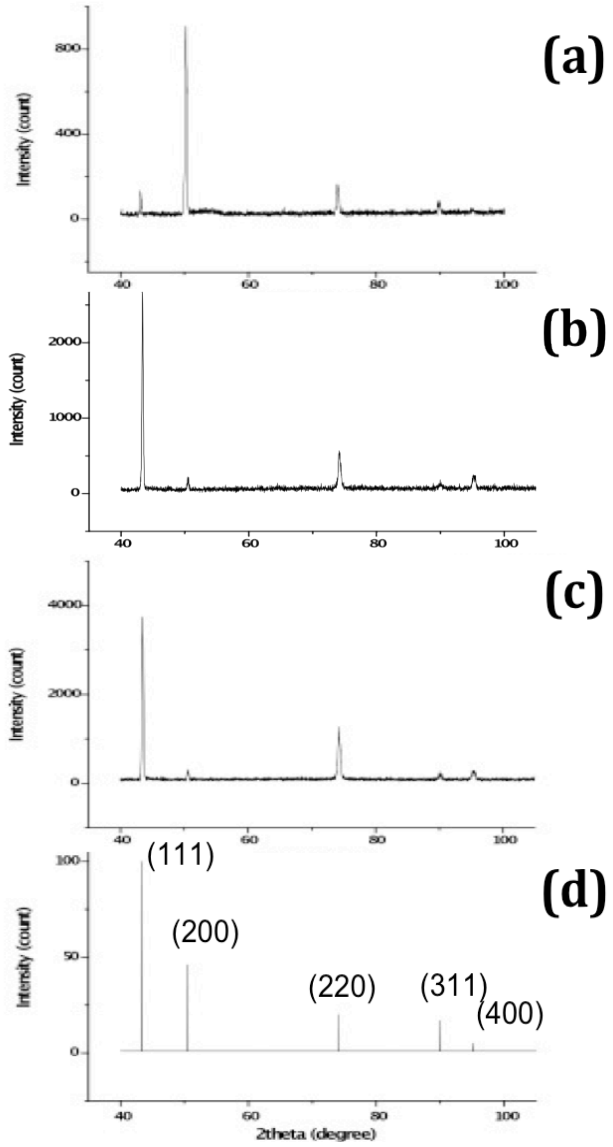

Figure 3.9. XRD patterns of copper nanowire arrays prepared at different electrodeposition potentials. (a) Copper nanowires prepared at -0.2 V with preferred orientation of (200); Copper nanowires showing preferred orientation of (111) and (220) prepared at (b) -0.4 V; and (c) -0.6 V; (d) Cu-JCPDS pattern for comparison. The electrodepositions were all carried out in 0.2 M $CuSO_4 \cdot 5H_2O$ and 0.1 M H_3BO_3 aqueous solutions with pH=4.0 for 1.5 hr.

The crystalline structures of as-prepared copper nanowire arrays embedded in AAO were analyzed by XRD, and TEM was used to study individual nanowires released after the template was dissolved by 0.1 M NaOH aqueous solution. Figure 3.9 shows the XRD results of nanowires prepared at different

potentials. When the potential was set constantly as -0.2 V, the (200) growth orientation is mostly preferred compared with the standard copper X-ray diffraction pattern Cu (JCPDS, 04-0836). At -0.4 V, copper nanowires showed polycrystalline structures but the (220) peak is higher than it is in the standard copper diffraction pattern. When the more negative potential of -0.6 V is applied, the (220) peak intensity is even larger in the corresponding XRD results.

In order to quantify preferred crystallographic orientation, texture analysis has been done. The textured coefficients (TCs) of preferred orientation were determined by the Harris formula [17]:

$$TC(hkl) = \frac{\frac{I_j(hkl)}{I_0(hkl)}}{N^{-1}\sum_{j=1}^{N}\frac{I_j(hkl)}{I_0(hkl)}} \qquad (3)$$

In which TC (hkl) is the texture coefficient of the (hkl) plane, *I (hkl)* is the measured relative intensity of the (hkl) plane, I_0 *(hkl)* is the relative intensity of the corresponding plane given in JCPDS data, and N is the reflection number, which stands for the total number of diffraction planes taken into account for calculations and represents the maximum value of the texture coefficient of the sample [3]. For TC (hkl) > 1, a preferred crystallographic orientation perpendicular to the (hkl) planes exists.

The calculated texture coefficients of the (111), (200), and (220) planes are shown in Figure 3.10 (a)-(c), respectively. It is seen that at the least negative value of -0.2 V, the copper nanowires grow highly orientated along the [200] with TC(200) achieving 2.2. When a more negative potential is applied at -0.4 V,

(111) and (220) are slightly preferred, from 0.15 and 0.78 to 1.38 and 1.37, together with a decrease of TC(200) from 2.2 to less than unity, 0.246. As the potential is further increased to -0.6 V, TC(220) becomes even larger, showing a more preferential orientation of (220) with a TC value of 1.76.

From Figure 3.10 (a)-(c), when lower potential (-0.2 V) was applied, the (200) growth plane is preferred. As the potential increases from -0.4 V to -0.6 V, the (111) plane becomes enhanced and polycrystalline character appears in Figure 3.10 (c). To explain the formation mechanism of electrochemically deposited nanowires, two-dimensional (2D) and three-dimensional (3D) nucleation growth mechanisms have been applied for characterizing the formation mechanism of electrodeposited nanowires [14, 16, 18]. The 2D mechanism involves the growth of existing nuclei, and the 3D mechanism entails nucleation followed by the formation of new copper grains [11]. In these models, a critical dimension N_C determines when new grains will grow during the deposition. Since N_C is inversely related with applied potential, at lower overpotential, larger critical dimension is predicted and consequently single-crystal nanowires can be obtained. From an energy point of view, the crystalline plane with low surface energy has more probability to be deposited to meet the principle of minimum free energy, values of which are 1.952 $J{\cdot}m^{-1}$, 2.166 $J{\cdot}m^{-1}$, and 2.237 $J{\cdot}m^{-1}$ for planes of (111), (200) and (220), respectively [19]. Therefore, the most densely packed (111) plane of Cu has most possibilities to appear in the XRD patterns.

The reported effects of applied potentials on textures of nanowires are diverse. Gao et al.[7] investigated the fabrication of Cu NWs from an almost neutral copper sulfate-boric acid aqueous electrolyte solution, claiming that low cathodic overpotentials are necessary to prepare monocrystalline copper nanowires growing along the (111) plane, which is consistent with the minimization of surface energy. Different results were reported by Thongmee et al.[20], giving the conclusion that single-crystal Cu nanowires with (220) orientation could be produced by potentiostatic electrodeposition at relatively high deposition potential (-2.0 V (SCE)), whilst potentials lower or higher than -2.0 V (SCE) resulted in polycrystalline nanowires. However, the results of the present study shown in Figure 3.9 and Figure 3.10 reveal that the (200) texture was preferred at lower potential and the preference for (111) texture increased with applied potential. One possible explanation for the observations here is the effect of H ion adsorption. It has been reported that the adsorption of H ions can diminish the surface energy, and further that high-energy surfaces are the preferred sites for the adsorption of H ions [3, 21, 22]. This effect increases the preference for high-energy (110) planes relative to low-energy (111) planes with the increase of overpotential or current density [22, 23], which are believed to accelerate the hydrogen adsorption process. However, the overpotential could also play opposite roles on the adsorption of H ions. It was reported by J. L. Duan et al.[3] that high overpotential could promote the hydrogen adsorption, while low overpotential could inhibit adsorption. The potential range of (-0.2 V to -0.6 V) in the present study was much lower than the potential applied in their

works (the absolute value was greater than 1 V), thus under our conditions the adsorption of H ions was possibly enhanced and the high-surface-energy plane of (200) was obtained.

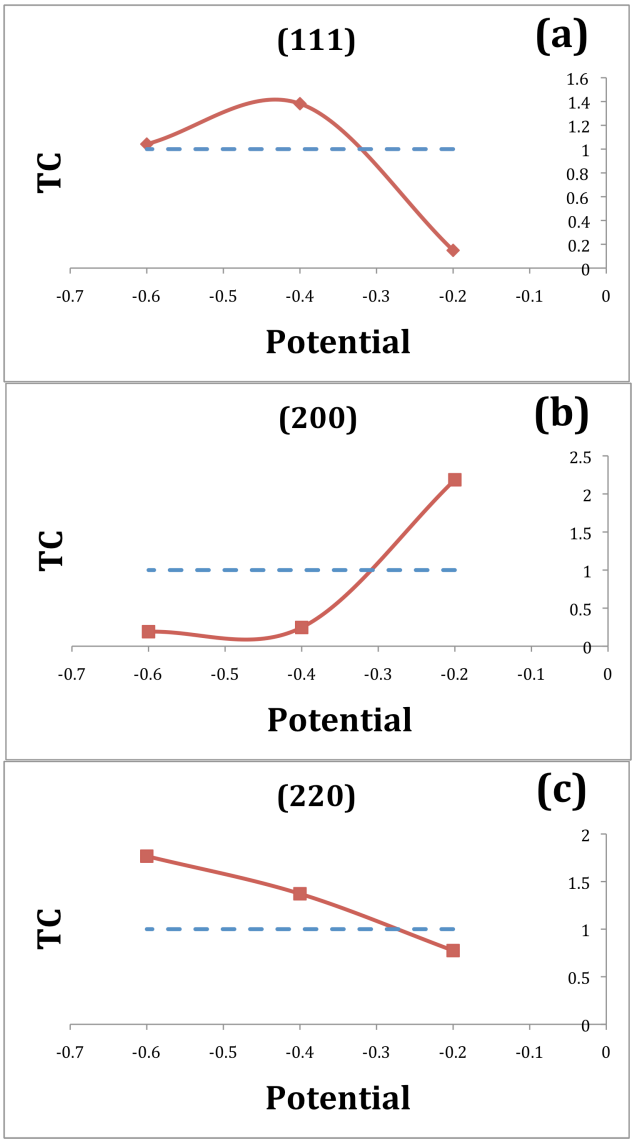

Figure 3.10. XRD patterns and calculated texture coefficients of (a) (111); (b) (200); and (c) (220) planes of Cu nanowire arrays deposited at varied electrodeposition potential -0.2 V, -0.4 V and -0.6 V in electrolytes with 0.2 M $CuSO_4 \cdot 5H_2O$ and 0.1 M H_3BO_3 aqueous solutions with pH=4.0 for 1.5 hr. Lines are a guide to the eye.

Highly magnified TEM images in Figure 3.11 show that the individual copper nanowires are dense, continuous, and uniform in diameter along their entire length. Additionally, there were no obvious differences between the morphologies of the individual copper nanowires formed at different applied potentials (−0.2 V, −0.4 V, and −0.6 V) because AAO templates with the same geometrical characteristics were used in each case.

Figure 3.11 presents the TEM image of the as-synthesized copper nanowires after being released from the AAO templates. Nanowires synthesized at all chosen potentials are shown to be single crystalline according to the SAED patterns from the insets of Figure 3.11 (a) to (f). When -0.2 V was applied, the growth plane of (111) presented in Figure 3.11 (a) and (b) is shown to be the preferred. However, the results do not correspond with the above XRD results of the nanowire arrays embedded in AAO, which show the strongest diffraction peak as (200). This could be explained by the random selection of individual nanowires that may not represent the crystallinity of the nanowire arrays embedded in the AAO membrane. Post-deposition annealing and selection bias may also play a role. For example, the selection may be affected by template etching and sonication used as the sample preparation for TEM characterization. In Figure 3.11 (c) and (d), the electron diffraction shows both (111) and (220) are observed when the potential of -0.4 V is applied during electrodeposition.

Unlike the lower potential data, the TEM data for more negative potentials are similar to XRD results, which show both (111) and (220) are preferred orientations. The TEM data also demonstrates copper nanowires with

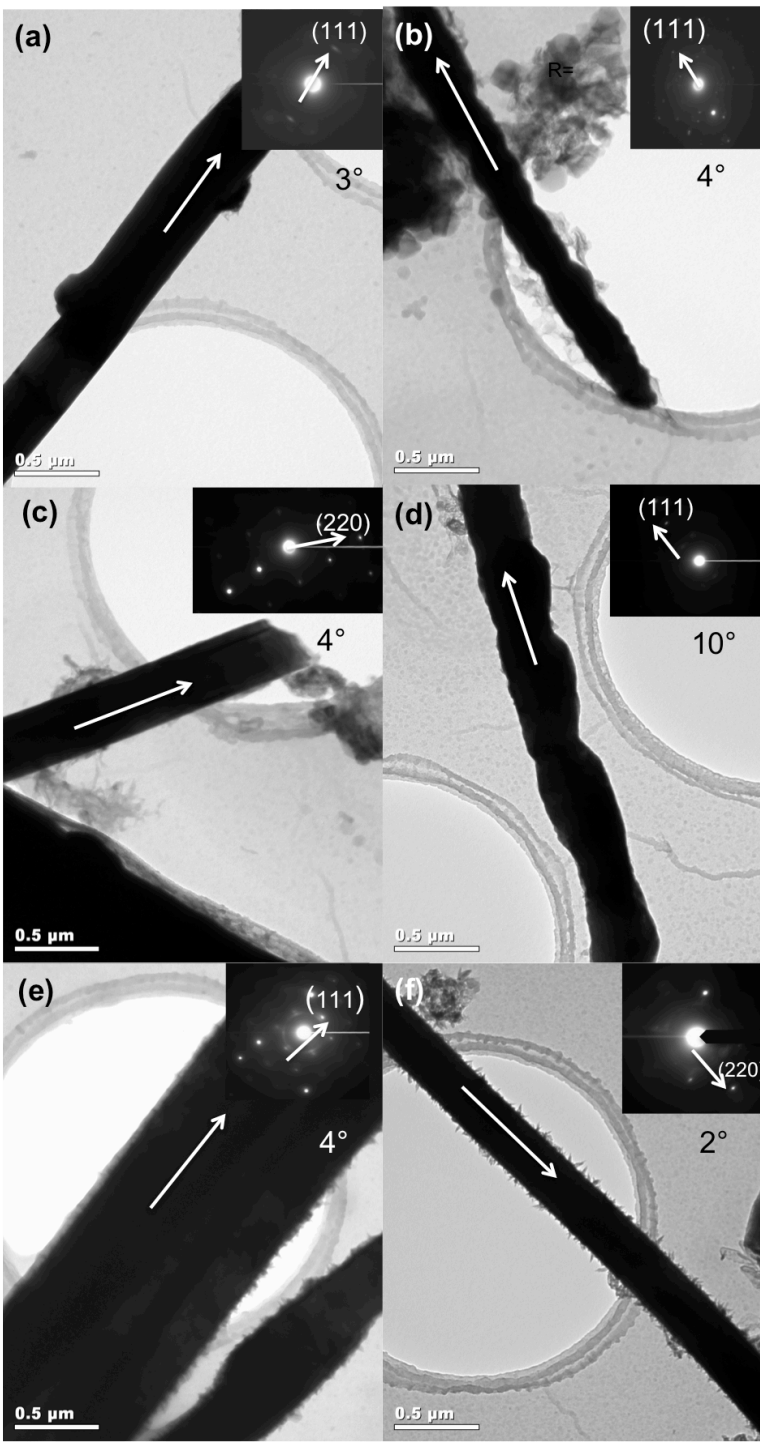

Figure 3.11. Preferential orientations of copper nanowires prepared at various electrodeposition potentials using potentiostatic method. The bright field TEM and SAED were performed for nanowires prepared at -0.2 V (a) and (b), -0.4 V (c) and (d) and -0.6 V (e) and (f) in electrolytes with 0.2 M $CuSO_4 \cdot 5H_2O$ and 0.1 M H_3BO_3 aqueous solutions with pH=4.0 for 1.5 hr. The nanowires are shown to be single crystal from SAED with different orientations.

single-crystal textures of (111) and (220) respectively in Figure 3.11 (e) and (f), corresponding to the XRD in Figure 3.9 (c) and the calculation results in Figure 3.10 as well. There is a small rotation angle from the nanowire growth direction to the (111) direction in Figure 3.11 (d) of 10°. This orientation is also observed for other SAED patterns in Figure 3.11 but less easy to be observed. The same phenomena was found previously where the intensity of individual spots of the SAED pattern of Au nanowires show a slight variation, which means that the nanowire is a single crystal with a slight structural deformation along its length [14]. Another possible reason could be the uneven positioned nanowires during preparation of the TEM sample, causing each individual nanowire to be not parallel to the surface of TEM grid and the rotation angle of crystalline orientations. However, the explanations are still incomplete and this topic needs to be explored in the future work.

3.2.2 Crystallinity of Copper Nanowires in Various Electrolytes

To obtain Cu nanowires with preferred growth orientations along the [111], [200], and [220] directions, electrodeposition parameters in relation to the bath conditions were also investigated. These include electrolyte concentration and solution pH value [6].

Using the potentiostatic mode and deposition potential at -0.4 V, the $CuSO_4 \cdot 5H_2O$ concentration of electrolyte was adjusted to 0.1 M, 0.2 M, and 0.3 M with 0.1 M H_3BO_3 added, and pH adjusted with addition of 0.1 M H_2SO_4. The electrodepositions were all carried out for 1.5 hr at room temperature. The textures of copper nanowire arrays were characterized by XRD to define the

preferential orientations. XRD results are shown in Figure 3.12 (a)-(c). Figure 3.12 (a) presents the polycrystalline nature of nanowires synthesized in a bath with 0.1 M $CuSO_4 \cdot 5H_2O$, which is the lowest concentration among the three experiments. Figure 3.12 (b) and (c) show that the orientation of (220) slightly

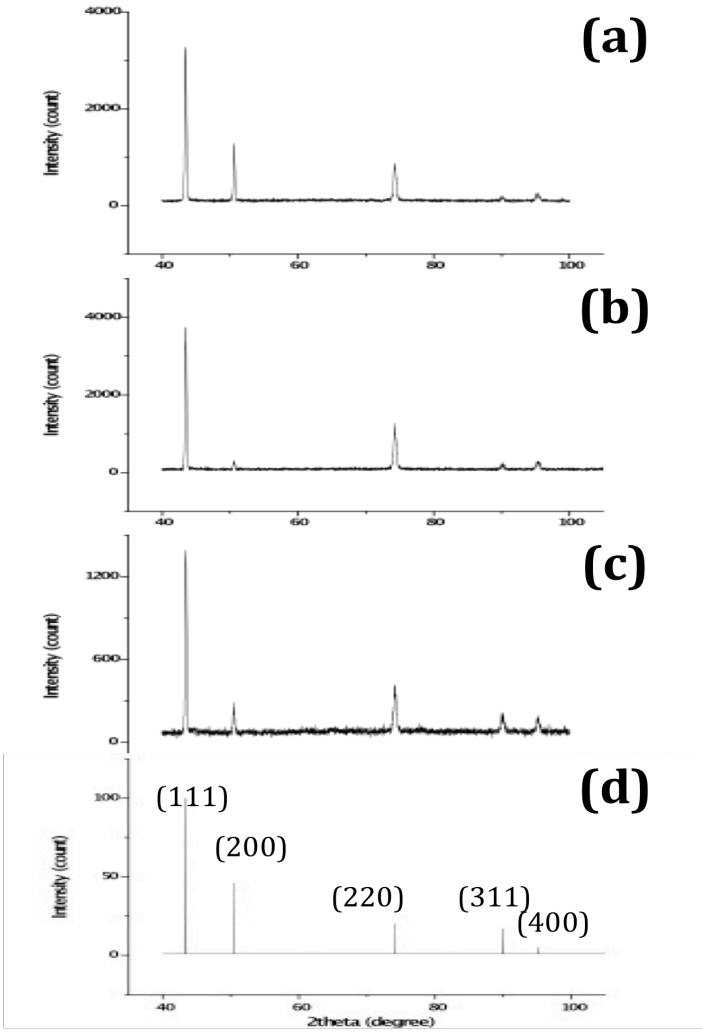

Figure 3.12. XRD patterns of copper nanowire arrays prepared in different electrolyte conditions: (a) Copper nanowires prepared in 0.1 M $CuSO_4 \cdot 5H_2O$ without preferential crystallinity; Copper nanowires showing preferred orientation of (111) and (220) prepared in electrolyte with (b) 0.2 M; and (c) 0.3 M $CuSO_4 \cdot 5H_2O$; (d) Cu-JCPDS pattern for comparison. All electrodepositions took place at constant potential of -0.4 V for 1.5 hr in electrolytes with 0.1 M H_3BO_3 and pH=4.0.

increases as the concentration increases compared to the ratio of peak intensity in the standard Cu JCPDS pattern.

After calculation by the Harris Formula, the texture coefficients for the (111), (200), and (220) planes are shown in Fig 3.13 (a)-(c), respectively. As

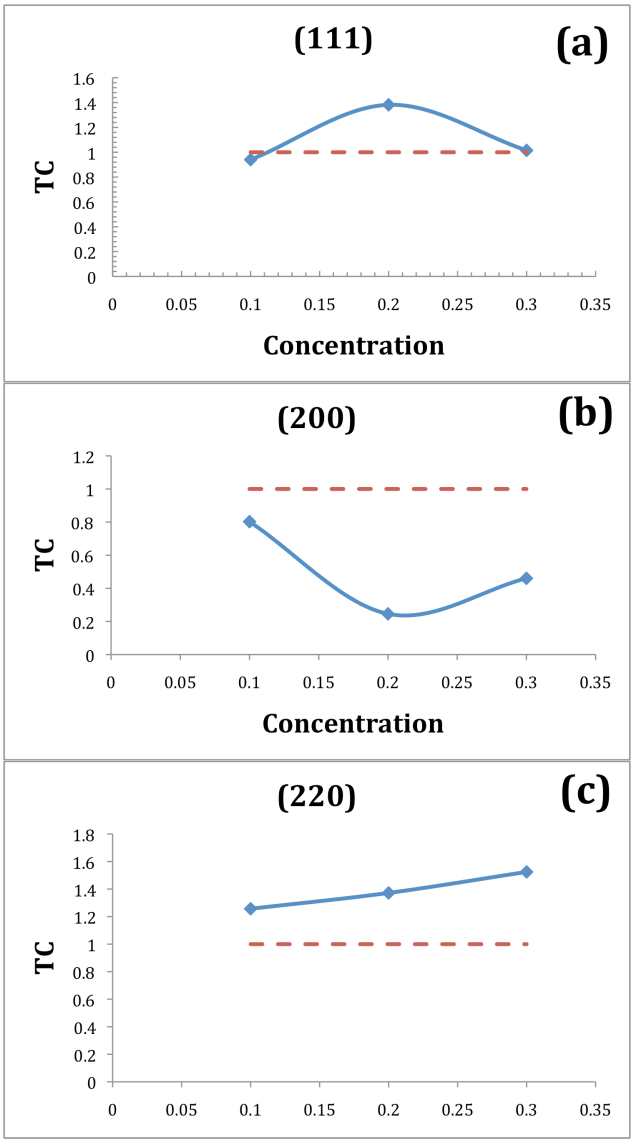

Figure 3.13. Calculated texture coefficients of (a) (111); (b) (200); and (c) (220) planes of Cu nanowire arrays deposited in bath of various $CuSO_4 \cdot 5H_2O$ concentrations of 0.1 M, 0.2 M and 0.3 M with same concentration of 0.1 M H_3BO_3 and pH=4.0, at constant potential of -0.4 V for 1.5 hr.

shown in Fig. 3.13 (a), the growth direction of [111] becomes more preferred when the concentration of $CuSO_4 \cdot 5H_2O$ is increased from 0.1 M to 0.2 M, indicated by the TC(111) increasing from 0.94 to 1.38. However, the orientation of (200), with the TC(200) always below unity, is not favored during the growth

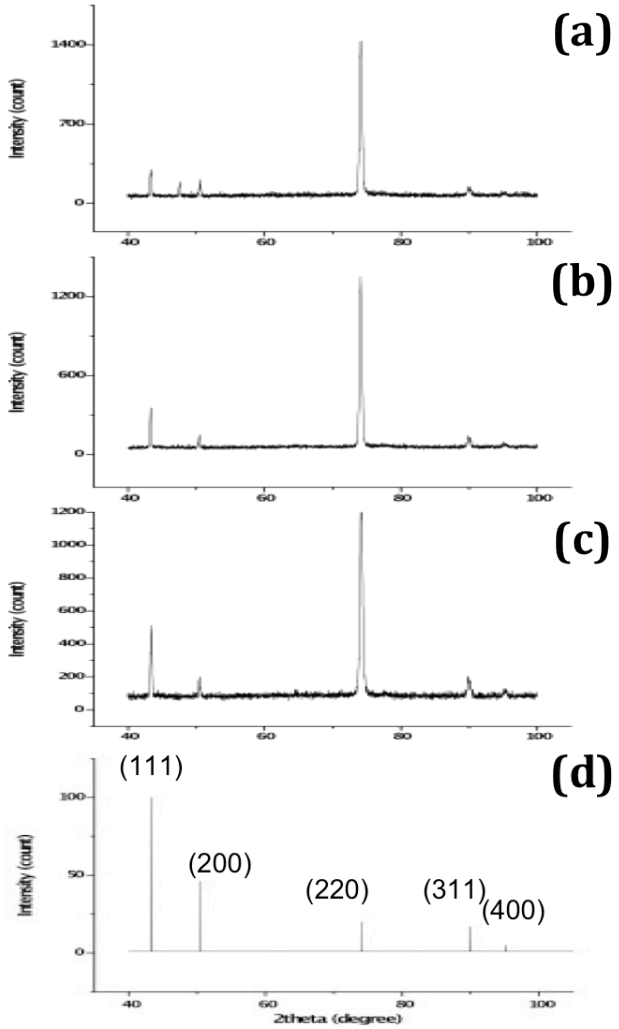

Figure 3.14. XRD patterns of copper nanowire arrays prepared in electrolytes with various pH values. Copper nanowires prepared in electrolytes with (a) pH=4; (b) pH=2.5; and (c) pH=1; (d) Cu-JCPDS pattern for comparison. All electrodepositions took place in electrolytes with 0.2 M $CuSO_4 \cdot 5H_2O$ and 0.1 M H_3BO_3 at constant potential of -0.2 V for 3 hr.

with concentrations from 0.1 M to 0.3 M. And, (220) is favored at all concentrations because the TC(220) stays above unity. The favor of (220) is positively correlated with the concentration of $CuSO_4 \cdot 5H_2O$ in the electrolyte. At lower concentration and a moderately higher potential, the growth process is nearly a thermodynamic equilibrium state, so Cu nanowires will grow along the [111] direction to meet the minimum of the surface energy [6]. However, in more highly concentrated solutions, growth is faster, inhibiting the approach to minimum surface energy [6]. As a result, the (220) crystal plane with higher surface energy appears. Thus, with higher concentrations of Cu^{2+}, and faster growth, it becomes more likely for nanowires to grow along high surface energy planes.

Not only the concentration of $CuSO_4 \cdot 5H_2O$ can affect the texture of copper nanowires, but also the acid concentrations represented by the value of pH, are able to affect different textures of nanowires [3, 6]. To study the influence of pH on the texture of copper nanowires, pH was adjusted to 4, 2.5, and 1 by adding different amounts of 0.1 M H_2SO_4 with the other electrodeposition parameters held constant. With applied voltage of -0.2 V, the pH variation experiments were conducted potentiostatically in electrolytes with 0.2 M $CuSO_4 \cdot 5H_2O$ and 0.1 M H_3BO_3 for 3 hr at room temperature.

XRD results are presented in Figure 3.14. The plot of calculated texture coefficients vs. pH are provided in Figure 3.15. It is evident in Figure 3.15 (a) and (b) that both the TC(111) and TC(200) are below unity when pH in the bath is adjusted from 1 to 4. In Figure 3.15 (c), TC(220) increases from 2.6 to

2.7 as pH goes from 2.5 to 4, and is above unity for all pH values, demonstrating that the (220) growth orientation of copper nanowires is preferred in each case with small sensitivity to pH.

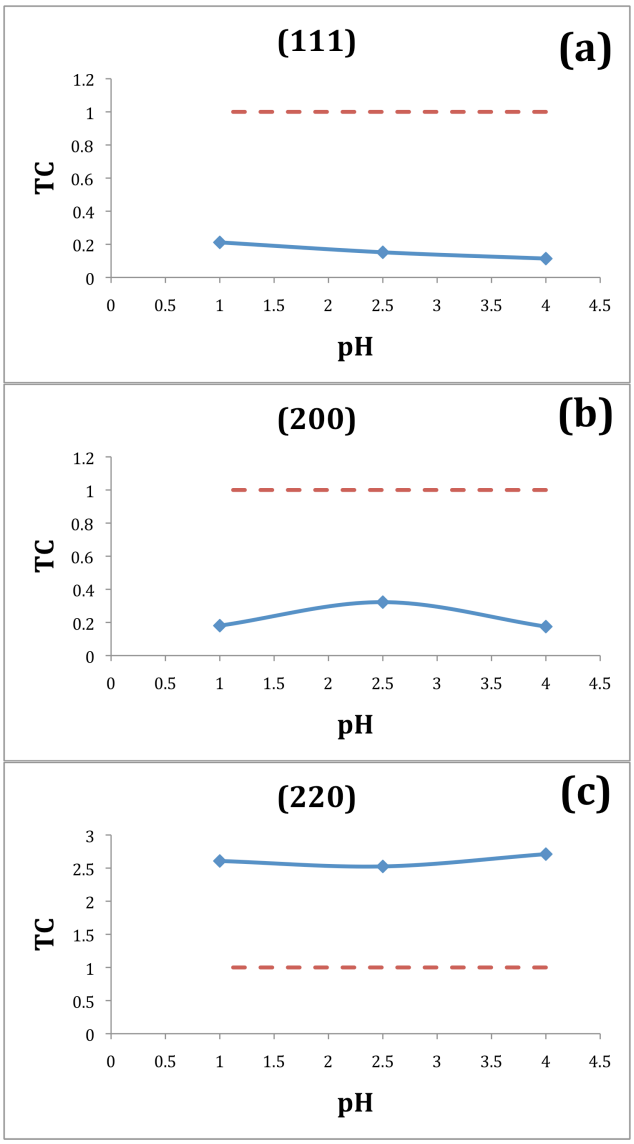

Figure 3.15. Calculated texture coefficients of the (a) (111); (b) (200); and (c) (220) planes of Cu nanowire arrays deposited in bath of various pH value of pH=4, 2.5 and 1 respectively. All electrodepositions took place in electrolytes with 0.2 M $CuSO_4 \cdot 5H_2O$ and 0.1 M H_3BO_3 at constant potential of -0.2 V for 3 hr.

The results in this study demonstrate that single-crystal copper nanowires with [220] direction could be obtained at a relatively low applied potential and high pH environment. When more H ions exist in the solution (higher pH), the [111] direction was also slightly enhanced, but dominated by the (220) diffraction peak. Results in Figure 3.14 (a) are consistent with Zhou et al.'s work [6] that copper nanowires with the [110] preferred orientation are synthesized when the pH value is about 2.5-3, which is a relatively high pH value. The effect of H ions via added sulfuric acid aqueous solution into the electrolyte is to increase the conductivity of the solution and stabilize high-surface-energy crystalline planes via adsorption [3]. The increase of conductivity decreases resistivity of the electrolyte, thus increasing the effective applied potential during electrodeposition, as per $U_{effective} = U_{real} - U_{electrolyte}$. Accordingly, low pH values not only increase the number of H ions that benefits the [220] growth direction by diminishing its surface energy, but also enhance $U_{effective}$ that promotes the formation of polycrystallinity, with [111] preferred [3], similar to increasing the applied potential to grow nanowires along the [111] direction to meet the minimum of surface energy[6]. In that case, there is a competitive process when adding more H ions in the electrolyte solution, which gives rise to the decreasing of TC(220) and increasing of TC(111) and the coexistence of the diffraction peaks of both (220) and (111) orientations as pH is lowered from 4.0 to 1.0, shown in Figure 3.15.

A comparison between Figure 3.9 (a) and Figure 3.14 (a) shows an inconsistent result of the preferred orientation of nanowires synthesized at the

same experimental conditions except for the deposition time, which is 1.5 hr in Figure 3.9 (a) and 3 hr in Figure 3.14 (a). The preferential crystalline plane of (200) is observed in Figure 3.9 (a) and that of (220) is presented in Figure 3.14 (a). According to previous results, increasing the Cu layer thickness leads to a change of the preferential orientation towards (220) texture, which is related to a stress relaxation [24]. Also, in the case of gold nanowires, surface stress can drive an fcc gold nanowire with an initial (100) orientation to reorient into an fcc nanowire with a (110) orientation [25]. In the references, the authors developed a simulation model and observed that a fcc (100) nanowire transforms into a body centered tetragonal (bct) nanowire because of surface stress and thermal vibrations, followed by the bct nanowire transforming into a fcc (110) nanowire due to shear. These phenomena may explain the inconsistency of the crystal orientation observed in this study. Clearly, this annealing effect may have implications for controlling the crystal structure of long wires, and needs to be further investigated.

3.2.3 Crystallinity of Copper Nanowires at Constant Currents

As an alternative to the potentiostatic technique, a constant current could be applied during electrodeposition to synthesize copper nanowire arrays (galvanostatic technique). Choosing a current of -0.7 mA, -1.5 mA, and -3.0 mA for electrodeposition for 3 hr at room temperature, copper nanowire arrays were fabricated in electrolytes of 0.3 M $CuSO_4 \cdot 5H_2O$ and 0.1 M H_3BO_3, with pH=4 adjusted by adding 0.1 M H_2SO_4. The potentials observed when applying -0.7

mA, -1.5 mA, and -3.0 mA were -0.01 to +0.01 V, -0.04 to -0.1 V and -0.06 to -0.1 V, respectively. Figure 3.16 (a)-(c) shows the crystallographic characteristics of nanowires synthesized using various constant currents. The growth orientations of (111) and (200) become more preferred as the applied current increases from

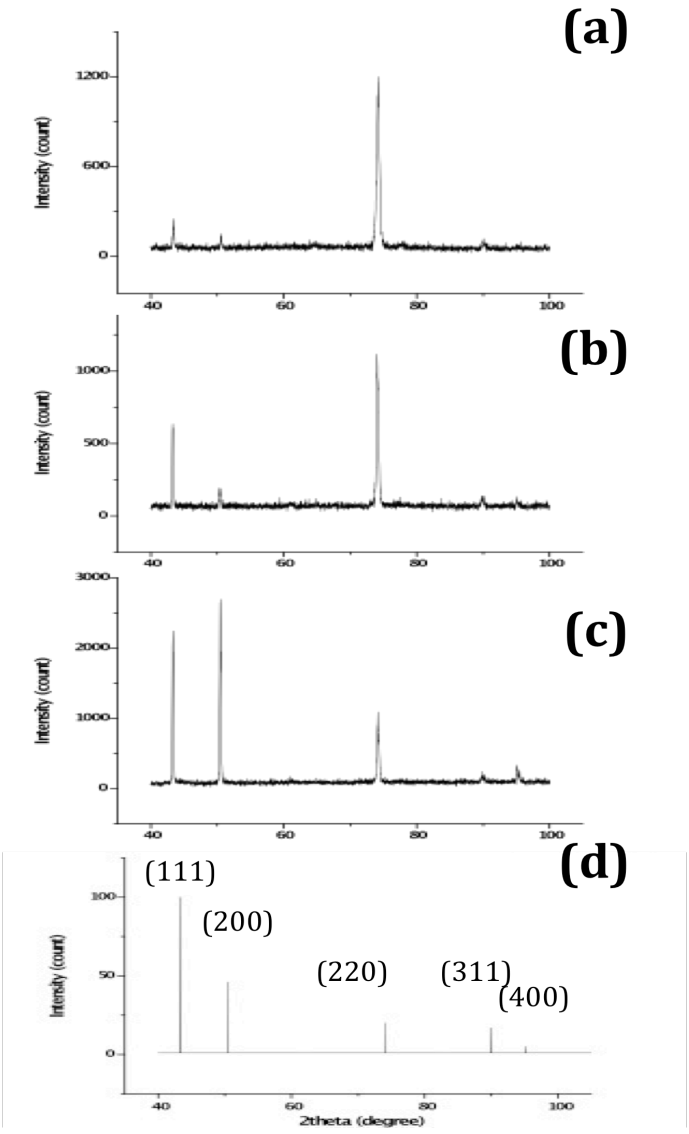

Figure 3.16. XRD patterns of copper nanowire arrays prepared by electrodeposition at various currents: a) -0.7 mA; (b) -1.5 mA; and (c) -3.0 mA; (d) Cu-JCPDS pattern for comparison. All electrodepositions took place in electrolytes with 0.3 M $CuSO_4 \cdot 5H_2O$ and 0.1 M H_3BO_3, pH=4.0 for 3 hr.

-0.7 mA to -3.0 mA. The growth direction of [200] becomes the most preferential when current is applied at -3.0 mA.

To further analyze the results, calculation was made based on the Harris Formula, the results of which are displayed in Figure 3.17. From Figure 3.17, copper nanowires show an almost single-crystal texture of (220) orientation when current is kept at -0.7 mA. As more negative current is applied, TC(220) decreased from 2.75 to 2.52, and finally reaches 1.2061 but still shows a small degree of preferred orientation of (220). It is seen that when applied current is more negative, nanowires present more polycrystalline characteristics. When a current of -3.0 mA is applied, the value of TC(200) increases from 0.13 to 1.21, showing a small preferential orientation of (200).

The factors discussed in Section 3.2.2 about the growth competition between [111] and [220] directions are further confirmed in Figure 3.16. In that section, [220] was observed as the preferred growth direction. Typical current density for applied voltage of -0.2 V was 12.5 mA/cm^2, as compared to the current density here from 3.5 mA/cm^2 to 15 mA/cm^2. [220] is demonstrated to be the preferred orientation when nanowires were grown in a high pH electrolyte with even lower current.

Concerning the relationship between current density and potential, the Tafel equation [5], $\eta = a + b\log j$, where $a = -2.3\frac{RT}{\alpha nF}\log j_0$ and $b = 2.3\frac{RT}{\alpha nF}$, gives insight. Note that *a* and *b* are constants at the same temperature and solution conditions. Therefore, electrodepositions at constant currents with fixed surface

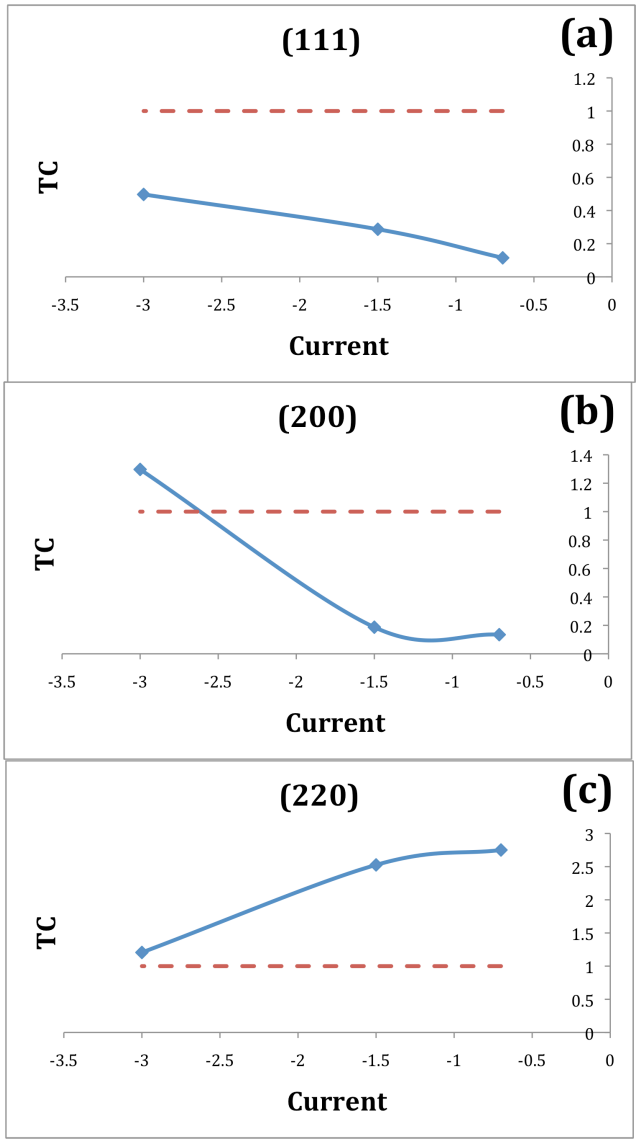

Figure 3.17. Calculated texture coefficients of (a) (111); (b) (200); and (c) (220) planes of Cu nanowire arrays deposited at various constant currents of -0.7 mA, -1.5 mA and -3.0 mA respectively. All electrodepositions were carried out in electrolytes with 0.3 M $CuSO_4 \cdot 5H_2O$ and 0.1 M H_3BO_3, pH=4.0 for 3 hr.

area of working electrodes should be characterized using the same mechanism as experiments in which the deposition was varied, but with more precise control of the grown structure of deposits. Therefore, the influences on the crystallographic characteristics by changing the constant currents in a range of current density of 3.5 mA/cm^2 to 15 mA/cm^2 were studied.

Since the current density observed during electrodeposition with constant potentials was as high as 32 mA/cm^2 for -0.6 V and 12.5 mA/cm^2 for -0.2 V as is seen in Table 3.5, the range of lower current density was selected to examine the crystallinity of copper nanowires. The results in Figure 3.16 (a) show that nanowires with a strong (220) orientation were obtained at an extremely low current density. As the value of the applied current goes up, (111) faceting increases and achieves its highest intensity in Figure 3.16 (c), which means the nanowires became polycrystalline at a relatively high deposition current, consistent with the growth mechanism discussed in Section 3.2.1 of this study. Moreover, as is shown in Table 3.5, the appearance of (200) orientation at -3.0 mA corresponds well with results shown in Figure 3.9 (a) and 3.10 (b), in which the (200) is the preferential orientation when electrodeposition was conducted for 3 hr at -0.2 V in an electrolyte with 0.2 M $CuSO_4 \cdot 5H_2O$.

Table 3.5. Preferred orientations at various current densities for potentiostatic and galvanostatic experiments.

Applied Current/Potential	-0.7 mA	-1.5 mA	-3.0 mA	-0.2 V	-0.4 V	-0.6 V
Current Density (mA/cm^2)	3.5	7.5	15	12.5	19.3	32
Preferred Orientation	(220)	(220)↓ (111)↑	(200)↑ (111)↑	(200)	(111)↑ (220)↑	(111)↓ (220)↑

3.3 References

1. Schlesinger, M.; Paunovic, M., *Modern Electroplating*. Fourth ed.; John Wiley & Sons, Inc.: 2000; p 888.

2. Konishi, Y.; Motoyama, M.; Matsushima, H.; Fukunaka, Y.; Ishii, R.; Ito, Y., Electrodeposition of Cu nanowire arrays with a template. *Journal of Electroanalytical Chemistry* **2003,** *559*, 149-153.

3. Duan, J.; Liu, J.; Mo, D.; Yao, H.; Maaz, K.; Chen, Y.; Sun, Y.; Hou, M.; Qu, X.; Zhang, L., Controlled crystallinity and crystallographic orientation of Cu nanowires fabricated in ion-track templates. *Nanotechnology* **2010,** *21*, 365605.

4. Toimil-Molares, M. E.; Brotz, J.; Buschmann, V.; Dobrev, D.; Neumann, R.; Scholz, R.; Schuchert, I. U.; Trautmann, C.; Vetter, J., Etched heavy ion tracks in polycarbonate as template for copper nanowires. *Nucl Instrum Meth B* **2001,** *185*, 192-197.

5. Bard, A. J. F., L. R., *Electrochemical Methods: Fundamentals and Applications*. John Wiley & Sons, Inc.: New York, 2001; p 833.

6. Zhou, W. F., G.; Li, X. ; Xu, S.; Chen, L; Wu, B.; Zhang, L., In Situ X-ray Diffraction Study on the Orientation-Dependent Thermal Expansion of Cu Nanowires. *J Phys Chem C* **2009,** *113*, 5.

7. Gao, T.; Meng, G. W.; Wang, Y. W.; Sun, S. H.; Zhang, L., Electrochemical synthesis of copper nanowires. *J Phys-Condens Mat* **2002,** *14*, 355-363.

8. Ebrahimi, F. B., G.R.; Kelly, M.S.; Matthews, T.E. , Mechanical Properties of nanocrystalline Nickel Produced by Electrodeposition. *NanoStructured Materials* **1999,** *11*, 8.

9. Inguanta, R.; Piazza, S.; Sunseri, C., Influence of the electrical parameters on the fabrication of copper nanowires into anodic alumina templates. *Applied Surface Science* **2009,** *255*, 8816-8823.

10. Riveros, G.; Gómez, H.; Cortes, A.; Marotti, R. E.; Dalchiele, E. A., Crystallographically-oriented single-crystalline copper nanowire arrays electrochemically grown into nanoporous anodic alumina templates. *Applied Physics A* **2004,** *81*, 17-24.

11. Toimil-Molares, M. E.; Buschmann, V.; Dobrev, D.; Neumann, R.; Scholz, R.; Schuchert, I. U.; Vetter, J., Single-crystalline copper nanowires produced by electrochemical deposition in polymeric ion track membranes. *Adv Mater* **2001,** *13*, 4.

12. Dresselhaus, M. S. L., Y.M.; Rabin, O.; Black, M.R.; Dressel-haus, G. , *Nanowires, In Springer Handbook of Nanotechnology*. 2007; p 1.

13. Dobrev, D.; Vetter, J.; Angert, N.; Neumann, R., Electrochemical growth of copper single crystals in pores of polymer ion-track membranes. *Appl Phys a-Mater* **1999,** *69*, 233-237.

14. Tian, M. W., J.; Kurtz, J.; Mallouk, T. E.; Chan, M. , Electrochemical Growth of Single-Crystal Metal Nanowires via a Two-Dimensional Nucleation and Growth Mechanism. *Nano Lett* **2003,** *3*, 5.

15. Maurer, F.; Brötz, J.; Karim, S.; Molares, M. E. T.; Trautmann, C.; Fuess, H., Preferred growth orientation of metallic fcc nanowires under direct and alternating electrodeposition conditions. *Nanotechnology* **2007,** *18*, 135709.

16. Gao, T.; Meng, G. W.; Zhang, J.; Wang, Y. W.; Liang, C. H.; Fan, J. C.; Zhang, L. D., Template synthesis of single-crystal Cu nanowire arrays by electrodeposition. *Applied Physics A Materials Science & Processing* **2001,** *73*, 251-254.

17. Harris, G. B., Quantitative Measurement of Preferred Orientation in Rolled Uranium Bars. *Phil Mag Lett* **1952,** *43*, 11.

18. Mohl, M.; Pusztai, P.; Kukovecz, A.; Konya, Z.; Kukkola, J.; Kordas, K.; Vajtai, R.; Ajayan, P. M., Low-Temperature Large-Scale Synthesis and Electrical Testing of Ultralong Copper Nanowires†. *Langmuir* **2010,** *26*, 16496-16502.

19. Vitos, L. R., A.V.; Skriver, H.L.; Kollar, J., The surface energy of metals. *Surface Science* **1998,** *411*, 7.

20. Thongmee, S.; Pang, H. L.; Ding, J.; Lin, J. Y., Fabrication and magnetic properties of metallic nanowires via AAO templates. *Journal of Magnetism and Magnetic Materials* **2009,** *321*, 2712-2716.

21. Sun, H.; Yu, Y.; Li, X.; Li, W.; Li, F.; Liu, B.; Zhang, X., Controllable growth of electrodeposited single-crystal nanowire arrays: The examples of metal Ni and semiconductor ZnS. *Journal of Crystal Growth* **2007,** *307*, 472-476.

22. Pan, H.; Sun, H.; Poh, C.; Feng, Y.; Lin, J., Single-crystal growth of metallic nanowires with preferred orientation. *Nanotechnology* **2005,** *16*, 1559-1564.

23. Wang, X. W.; Fei, G. T.; Chen, L.; Xu, X. J.; Zhang, L. D., Orientation-Controllable Growth of Ni Nanowire Arrays with Different Diameters. *Electrochemical and Solid-State Letters* **2007,** *10*, E1.

24. Serre, C. Y., N.; Martınez, S.; Perez-Rodrıguez, A.; Morante, J.R.; Esteve, J.; Montserrat, J. , Electrochemical deposition of Cu and Ni/Cu multilayers in Si Microsystem Technologies. *Sensors and Actuators A: Physical* **2005,** *123-124*, 633-639.

25. Diao, J.; Gall, K.; Dunn, M., Surface stress driven reorientation of gold nanowires. *Phys Rev B* **2004,** *70*.

Chapter 4 CONCLUSIONS AND FUTURE WORK

4.1 Summary and Conclusions

Copper nanowires with preferred crystalline orientations were successfully prepared by electrodeposition based on AAO templates with a range of experimental conditions. Using the potentiostatic technique, the applied potential, concentration of $CuSO_4 \cdot 5H_2O$, and pH value of electrolytes were varied to investigate the effects on crystallographic orientation of copper nanowires. The current and electrodepositing time were also selected as control variables when performing the galvanostatic technique to investigate the growth rate and crystalline structures, respectively. From SEM and TEM images, it can be observed that high densities of nanowires were grown into the pores of AAO templates and the geometry of the pores in templates determine the shape of the wires, which were mostly straight with smooth contours.

The growth rate of nanowires was found to be directly related to the deposition time, concentration of $CuSO_4 \cdot 5H_2O$, and the applied potential in Section 3.1. However, the calculated growth rates based on Faraday's Law were significantly larger than that measured by SEM images. These discrepancies in Table 3.1 were likely caused by the enlarged surface area of deposition caused by penetration of bath solution onto the gold-coated side and leakage currents. Coalesced films were observed on the top of the AAO after electrodeposition with long duration, demonstrating fully filled pores and grown nanowires as is shown in Figure 3.3 (c). Higher potential improved the length uniformity of the nanowire arrays when constant potentials were applied. Although higher deposition

potentials contribute to faster growth initially, there are two effects that may decelerate the nanowire growth so as to improve the length uniformity as is presented in Figure 3.7: bubbles generated in the concurrent hydrogen evolution blocking pores partially [1], and copper ion transport limitations to the electrode surface [2-4]. Both of these effects act to retard growth and enhance uniformity.

XRD characterizations provided in Figure 3.14 (a) and Figure 3.16 (a) show that copper nanowires with preferential orientation of (220) were obtained when using a higher pH electrolyte potentiostatically or a lower constant current density galvanostatically, respectively. A different preferred growth direction of [200] was identified when a less negative potential or current was applied as is shown in Figure 3.9 (a) potentiostatically, and in Figure 3.16 (c) galvanostatically. In Section 3.2.1, it is discussed that single-crystal nanowires could be formed when lower potential was applied because a 2D nucleation mechanism was more favored than 3D mechanism [5-7]. From an energy point of view, the crystalline plane with the minimum surface energy is most preferred during electrodeposition [8]. However, H ion adsorption can decrease the surface energy of high-energy planes and influence the preferred growth directions [9-11]. In addition, the inconsistency between preferential orientations in Figure 3.9 of this study and previous reports by Gao et al. [12] and Thongmee et al.[13] may be due to inconsistencies in potential ranges used, which in return affect the H^+ adsorption. As was discussed in Section 3.2.1, the low potential range decreases the H^+ adsorption and the high potential range increases the adsorption.

The pH value and applied potential influence the textures of nanowires via their effects on H ion absorption and consequently the crystalline planes' surface energy that ultimately dictates the growth orientation. There is a competitive process as was shown in Figure 3.14 and Figure 3.15 when more H ions are added to the electrolyte, which contributes to the decreasing preference of (220) and increase of (111) as pH is reduced, owing to the decrease of H adsorption and the increase of effective potential in electrolyte, respectively.

An inconsistency of crystalline orientation between Figure 3.9 (a) and Figure 3.14 (a) was observed when deposition time was the only variable. As explained earlier, a stress relaxation has been linked with a change of preferred orientation to (220) when increasing the copper layer thickness, suggesting that the (220) crystalline orientation may be preferred for thick layers due to stress effects [14, 15]. In the future experiments, instead of deposition time, lengths of nanowires will be included as of the control variables for more precisely control of the preferential orientations. Therefore, both thickness and H^+ adsorption effects appear to be important for nanowire crystalline orientation. In this work, both of these effects were found to enhance (220) and (200) orientation relative to the (111) orientation expected from general surface energy considerations. Conditions for [111] oriented growth were previously reported by Gao et al.[12]. They observed [111] preferential growth for copper nanowires in diameter of 60 nm at overpotential of -232 mV. However, in this work, the preference of [111] orientation was observed when potential larger than -400 mV was applied, using templates with larger pores. Different observations were made for [200] growth.

Riveros et al. [2] reported that copper nanowires were grown along [200] direction at the overpotential of -250 mV. In this work, with higher pH value and lower concentration of $CuSO_4 \cdot 5H_2O$, [200] growth was preferred when current density was between 12 – 15 mA/cm^2. The conditions are specified in Table 3.5. Moreover, (220) growth orientation was favored when either lower potential or highly concentrated electrolyte was employed, as is specified in Figure 3.13 (c) and Figure 3.17 (c). However, the comparison may not be completely valid because of different control variables selected, e.g. the concentration of $CuSO_4 \cdot 5H_2O$, the pH value, and the pore size of templates, which can also influence the crystalline structures of nanowires.

The results presented herein should be helpful not only in regard to templates synthesis of other metallic nanowires with preferred orientations, but also to applications concerning single-crystal metallic nanowires with functional performances via mechanical, electrical and magnetic properties.

4.2 Future Work and Preliminary Studies

For further investigation of the optimized conditions to prepare single-crystal copper nanowires, a few additional parameters affecting deposition are discussed. These include pore size effects, different solution chemistries, and the effect of stirring. The pore size of the templates may play an important role in electrodeposition. Previous results have demonstrated that the growth orientation of Ni nanowires turns from [110] to [111] with increasing diameter of nanowires based on the interface energy minimum principle [16]. Moreover, bismuth telluride nanowires with diameter of 25 nm show a strong (110) texture

differing from that of larger diameters [17]. In addition, the extension of the work to electron-tunneling devices fabricated with single-crystal nanowires will be discussed. In particular, we consider strategies to free the nanowires and disperse them onto a surface.

4.2.1 Electrodeposition of Copper Using Other Electrolytes

During electrodeposition, foreign species can be adsorbed on or co-deposited, affecting the electrodeposition process and, in turn, resulting in changes in the deposit texture [1, 18]. Thus, the texture of electrodeposits is sensitive to foreign species such as anions, organic additives, and even suspended particles[5].

4.2.1.1 Using Copper Chloride in Electrolytes

Chloride ions, one of the most extensively used additives for copper electroplating, are generally agreed to change the overpotential for copper deposition by adsorption on the cathode surface, thus affecting the texture of copper deposits. For preparation of copper nanowires, $CuCl_2 \cdot 2H_2O$ has previously been investigated as the source of deposited copper [19, 20]. In W. Shao et al.'s work, two competitive affects of chloride ions influencing copper deposition were concluded. At low concentration, chloride ions depolarize the Cu reduction process, while high concentrations induce complexation of copper species and cause a cathodic polarization of the deposition process [19].

As shown in Figure 4.1, copper and other metallic nanowires were synthesized from chloride solutions using AAO templates, but via redox reaction

instead of electrodeposition [20]. The aqueous solution of metal chloride salts (2 ml) was infiltrated into a Au-coated, Al-surrounded AAO template mounted in a simple polymethylmethacrylate (PMMA) holder to fabricate nanowire arrays from two ends based on nanochannel-confined growth. The method is energy saving and facile compared with electrodeposition and electroless deposition. However, the control of the crystallinity of nanowires may not be as good as with electrodeposition, because the electron transfer process in solution was

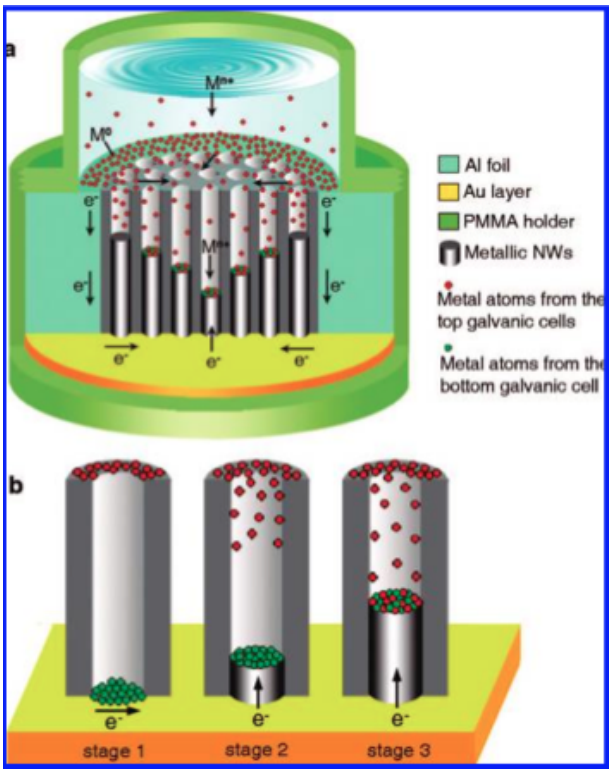

Figure 4.1. Schematic for the formation of Metal Nanowires (MNWs) inside vertically aligned nanochannels of Au-coated, Al-surrounded AAO templates. (a) The simple setup for the formation of the MNWs. (b) The detailed formation process of the MNWs[20].

spontaneous, and the deposition lasted too long (7 days for copper nanowires), which decreases the practicality of this approach. Nonetheless, the successful

synthesis of nanowires with metallic chloride solution expands the possibilities of preparing more metal materials, though studies concerning crystallographic properties still need to be explored.

4.2.1.2 Using Copper Nitrate in Electrolytes

Because of the varied atom arrangement with different crystal facets, it is known that the texture of the electrodeposits is mainly caused by different growth rates of differently oriented planes at a given overpotential [18]. The growth-rates of different planes may change with overpotential, resulting in changes in the deposit texture.

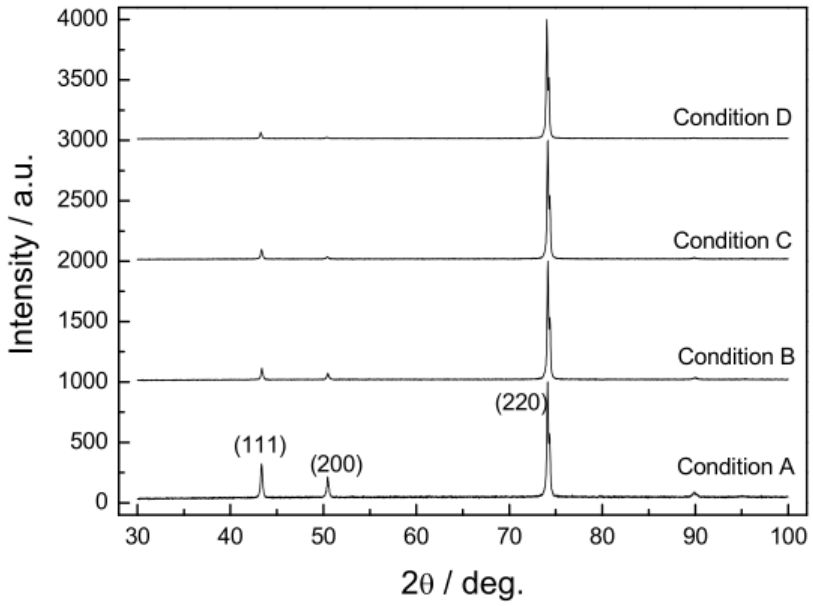

Figure 4.2. XRD patterns of copper coatings deposited in DC condition. All conditions are with 400 g/L $Cu(NO_3)_2 \cdot 3H_2O$. Condition A: 0 mg/L Cl^-; Condition B: 10 mg/L Cl^-; Condition C: 20 mg/L Cl^-; Condition D: 30 mg/L Cl^-[18].

Copper electrodeposition with only copper nitrate as the electrolyte was previously studied by others and their XRD results in Figure 4.2 show that the

deposited copper follow a preferred (220) texture, but not single crystalline based on the XRD pattern. However, as copper chloride was added to the electrolyte from 10 mg/L to 30 mg/L, the (111) and (200) peaks decreased and almost disappeared in the diffraction pattern, leaving a single peak of (220) and showing the single crystallinity. It was observed that chloride ion promotes the texture of this orientation.

4.2.2 Different Pore Sizes for Preparing Copper Nanowires

As a part of our preliminary studies, 10 x10 mm freestanding AAO square membranes (Synkera), with nominal pore diameter of 100 nm, pore density of 10^{11} cm^{-2} and thickness of 50 μm were also used as templates for copper nanowires synthesis.

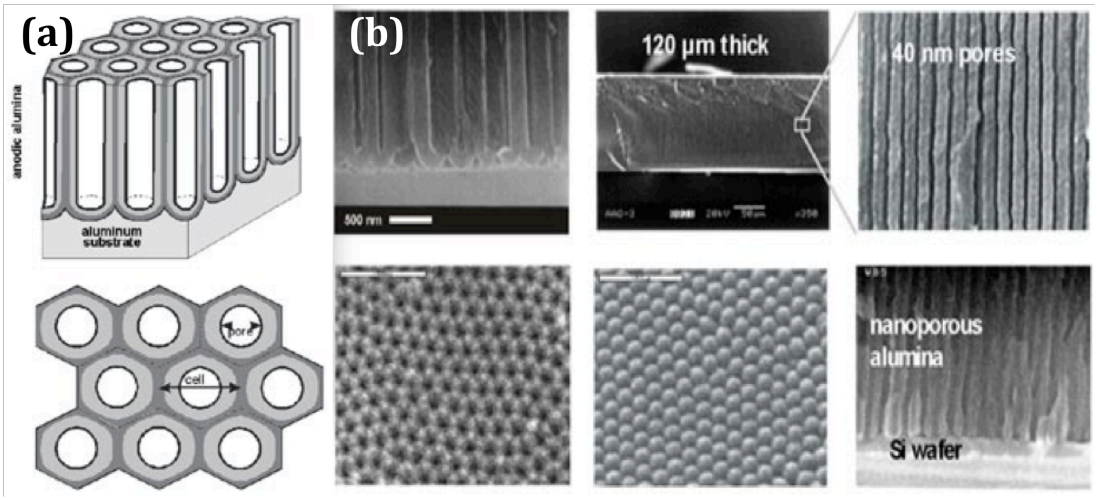

Figure 4.4. The drawing (a), and SEM images (b) of AAO with pore diameters of 40 nm and thickness of 120 μm. Different architectures of AAO are developed and used, including AAO attached to Al foil, free-standing AAO wafers and AAO nanotemplates integrated onto various non-Al substrates, such as Si wafers. [http://www.synkera.com/ceramic-membranes/symmetric-membranes.html]

Figure 4.4 is a drawing of the basic design of AAO with pore sizes of 40 nm in diameter. In Figure 4.4 (a), compared with the pore size, the distance between each pore is around the same as the pore diameter, which leads to thick walls among the pores and lower pore density of the membranes.

According to SEM images before and after filling the templates with copper in Figure 4.5, it is clearly seen that the pore density is larger for the 200 nm (Figure 4.5 (c)) than the 100 nm AAO templates (Figure 4.5 (a)), resulting in larger amount of nanowires grown inside the 200 nm samples (Figure 4.5 (d)). This is due to the thicker walls between channels of the AAO templates for the 100 nm pores.

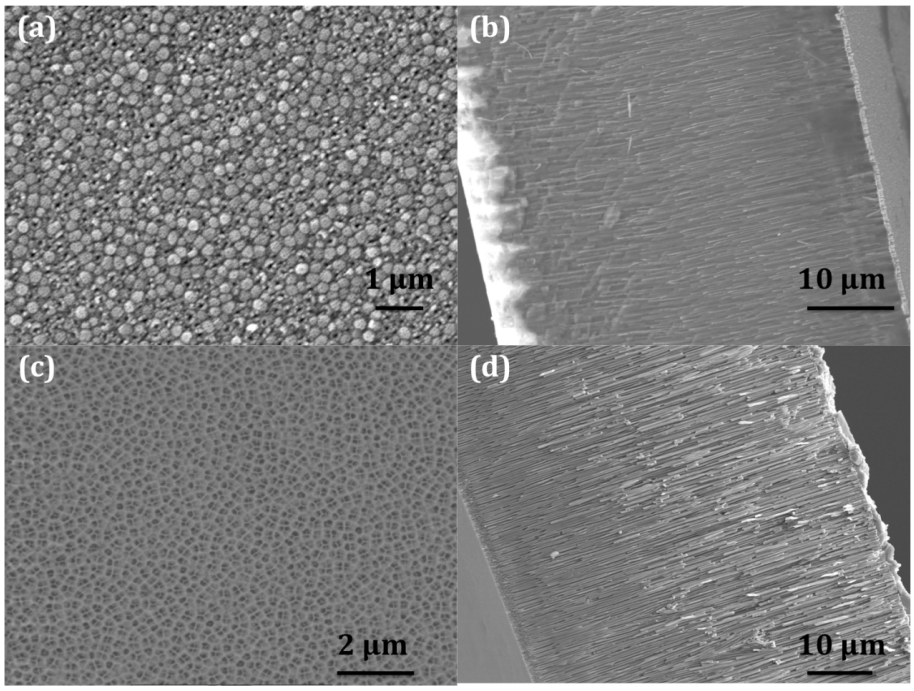

Figure 4.5. Comparison between AAO templates with 100 nm and 200 nm in diameter: (a) Plan view of AAO with 100 nm pore size after Au sputtering; (b) Cross-section of AAO with 100 nm pore size embedded with copper nanowires; (c) Plan view of AAO with 200 nm pore size; (d) Cross-section of AAO with 200 nm pore size embedded with copper nanowires.

It is more difficult for copper ions to diffuse into smaller pores during eletrodeposition. In that case, increasing the deposition potential, deposition time, and the concentration of copper ions in the bath can improve the growth rate of nanowires in the smaller structures.

An electrolyte was made from 30g/L (0.19 M) $CuSO_4 \cdot 5H_2O$ and 0.1 M H_3BO_3, in which the pH was adjusted to 4.0 by adding 0.1 M H_2SO_4 and measured using pH test papers. The galvanostatic method was employed to grow nanowires. In the beginning of the electrodeposition, a relatively large deposition current of -15 mA was applied for 10 min to enhance nucleation.

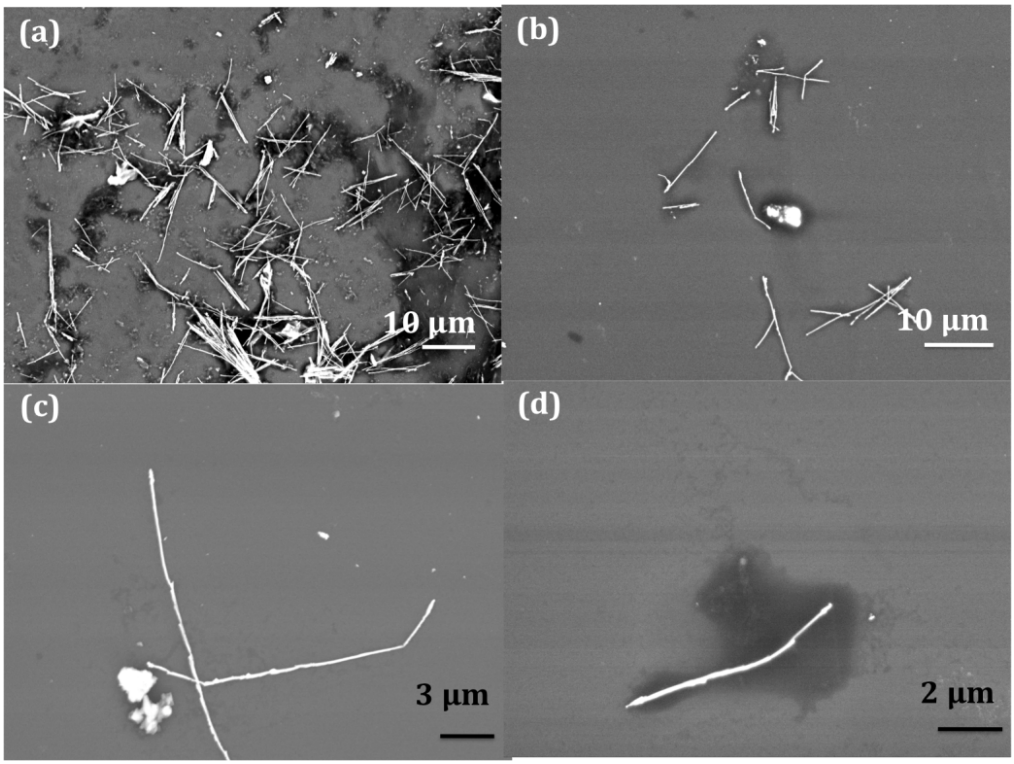

Figure 4.6. SEM images of copper nanowires synthesized based on AAO with 100 nm pores.

Subsequently, the current was decreased to -5 mA and maintained constant for 3 hrs. After removing the AAO template by dissolution, nanowires were dispersed and stored in ethanol. For further characterization, a drop of solution was placed on a Si/SiO_2 substrate.

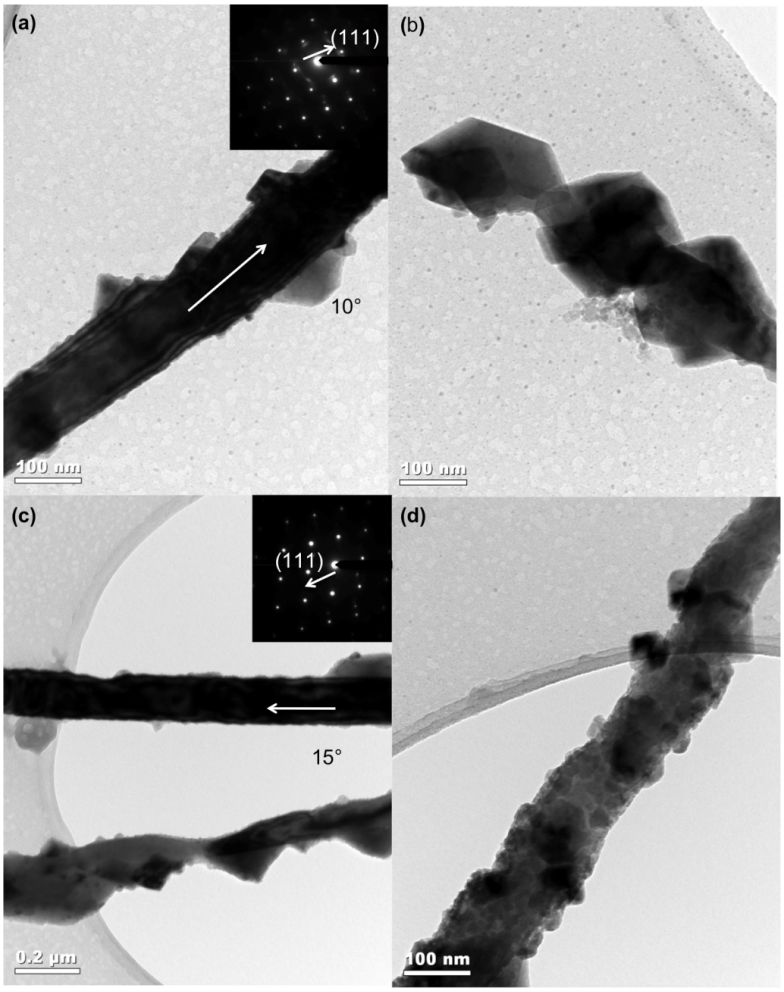

Figure 4.7. TEM images of the morphology and texture of 100 nm copper nanowires. Single crystallinity is shown along the [111] direction.

From the SEM images in Figure 4.6 (a)-(d), copper nanowires have the same diameter as pores in AAO. However, because of the smaller diameter,

nanowires appear more flexible after being released from templates and dispersed on the substrate, compared with the straight and rigid copper nanowires of 200 nm diameters.

The crystalline structure of 100 nm copper nanowires was further explored by TEM characterization. TEM results in Figure 4.7 show the diameter of each single nanowire is around 120 nm, which is 20 nm larger than the nominal pore size of AAO. The surface of the nanowire was not as smooth as the 200 nm ones but they had a single crystal texture along the [111] direction, demonstrating that single-crystal nanowires can be prepared based on templates with smaller pores.

The characteristics of the morphology with faceted crystallographic planes at its side walls rather than a cylindrical shape may relate to the low current density [3]. Other factors may be considered and studied in the future, such as the morphology dependence on smaller pore size and structure of the inside walls of the pores. Also, the template dissolution procedure needs to be improved to avoid residuals and impurities contained in the nanowire solutions, which are apparent in the SEM and TEM images.

4.2.3 Other Experimental Conditions during Synthesis

To optimize surface smoothness, size, and crystallinity of synthesized copper nanowires, more parameters during electrodeposition were explored. The treatment for samples after completion of the electrodeposition is also important because the uniformity of nanowires in solution is needed to avoid aggregation and protect the nanowires from being ruptured to undesired lengths.

4.2.3.1 Using a Stirrer During Electrodeposition

According to previous reports, most electrodeposition experiments are performed without stirring [21, 22]. M.Gupta, et al. proved that with stirring, copper nanowires and nanotubes were able to be grown in porous templates when different current pulses were applied. However, they did not analyze how stirring would affect the growth of nanowires. Jae Kwang Lee et al. have successfully synthesized nickel nanowires using electrodeposition with

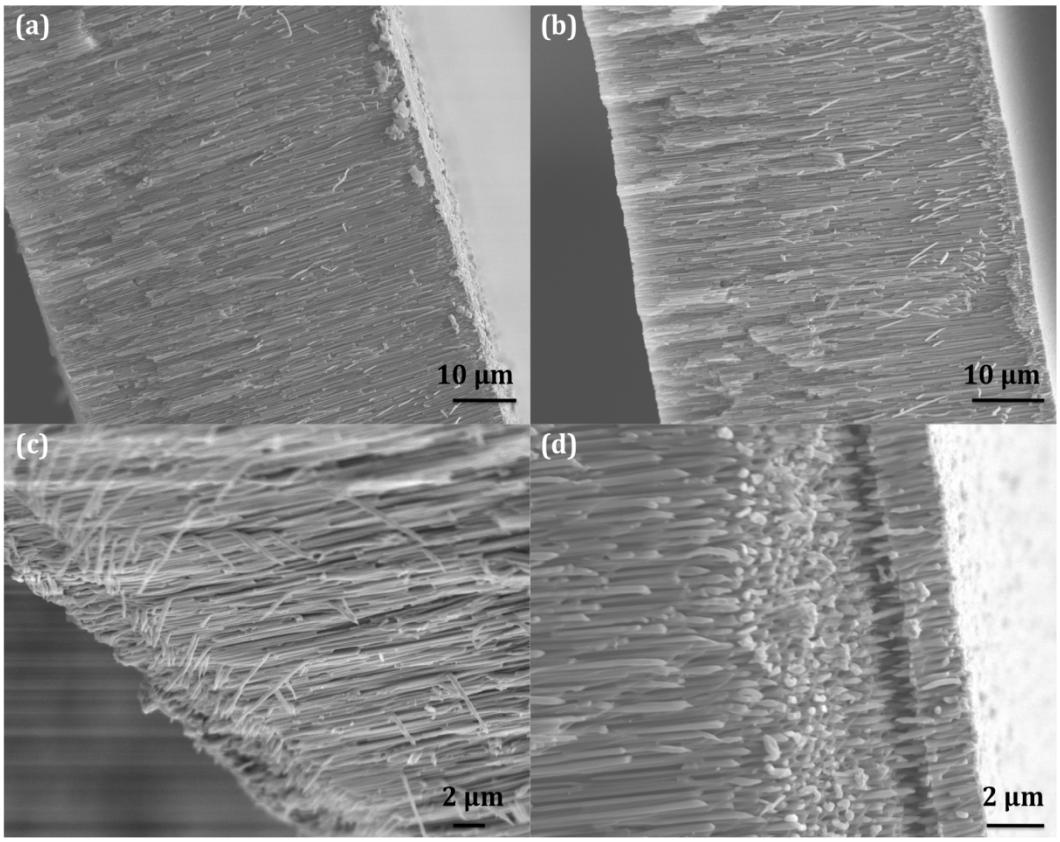

Figure 4.8. Comparison between copper nanowire arrays fabricated with and without stirring during electrodeposition. (a) Cross-section view of nanowires grown without stirring; (b), (c) and (d) Cross-section view of nanowires grown with stirring.

stirring and explained that the bubble layer was removed from the electrode surface and the potential was stable by stirring the solution during the electrodeposition [23].

In preliminary experiments, a stirrer was custom-made by cutting an ultrathin glass tube to get a 10 mm segment and heating to seal both openings to keep an iron wire inside. The same experimental conditions were applied as in Section 3.2.2.1, the bath contained 0.3 M $CuSO_4 \cdot 5H_2O$ and 0.1 M H_3BO_3 with pH=4, in which deposition was carried out potentiostatically with constant potential of -0.6 V for 1.5 hr with magnetic stirring at 350 rpm by putting the three-electrode cell on a hotplate (Isotemp, Fisher Scientific). A comparison of morphologies by SEM images is presented in Figure 4.8.

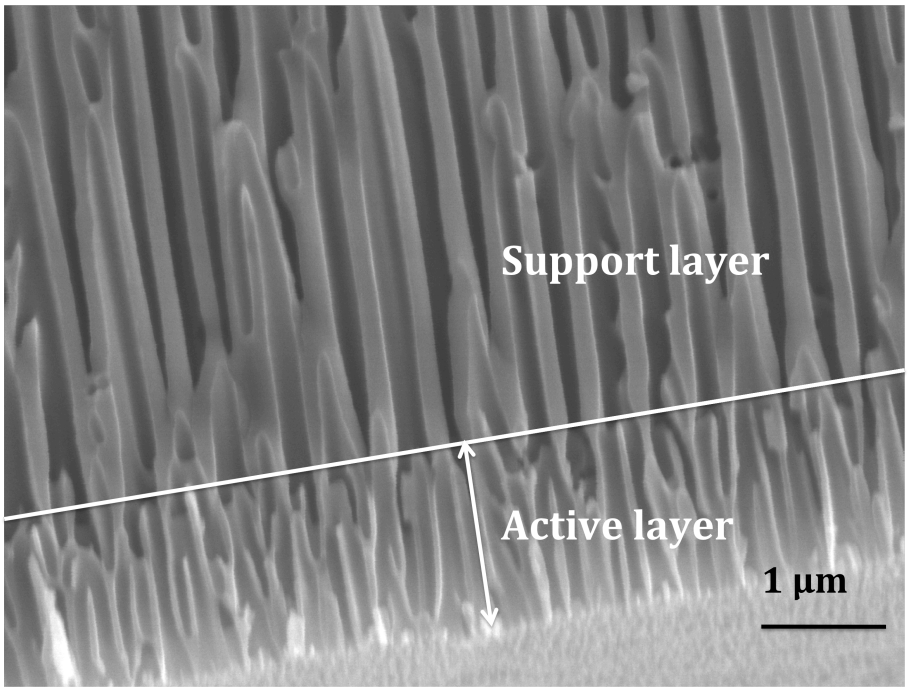

Figure 4.9. The SEM image of the pore structure and dimensions of an ANOPORE membrane with 100 nm pore diameter. The branched side (active layer): the thickness is ~1.5 µm with pore size of ~100 nm; the support layer: The thickness is ~58.5 µm with pore size of ~200 nm.

Characterized under similar magnification, nanowire arrays in Figure 4.8 (b) show a relatively higher filling density than in (a), which is further proved by (c) and (d) with larger magnification. Note that only the first 1.5-2 μm of the pores were 100 nm in diameter. The actual size of the remaining 58.5 μm of the membrane is compose only with 200 nm pores, as is shown in Figure 4.9, which was also reported in previous work [2, 24].

The rupture in (d) separating nanowires into two segments was induced by the large stress applied to the nanowires, which likely resulted from the suddenly change of pore diameters in that section of the membrane from 100 nm to 200 nm. Since it is found that grain boundaries are the preferred places to bend wires released from templates [10], further crystallographic studies could be focused on the changing of textures of nanowires in the area connecting the 100 nm and 200 nm pores.

4.2.3.2 Adding Thiols to Solution with Released Nanowires

1-Decanethiol is commonly used for separating gold nanoparticles and chemical functionalization of the surface of gold nanomaterials [25, 26]. It has also been reported that octadecanethiol reduces CuO to Cu^{+} by formation of a dithiol, which results in a multilayer copper thiolate complex that protects copper nanowires from being oxidized[27].

To better understand the effects of thiols, a preliminary experiment was carried out using SEM images to study nanowires. To isolate the released copper nanowires inside the ethanol solution, 0.1 M 1-Decanethiol was added to

the solution containing the nanowires with a pipette designed to handle 1-10 µL. Nanowires are prepared at the conditions described in the caption of Figure 3.14.

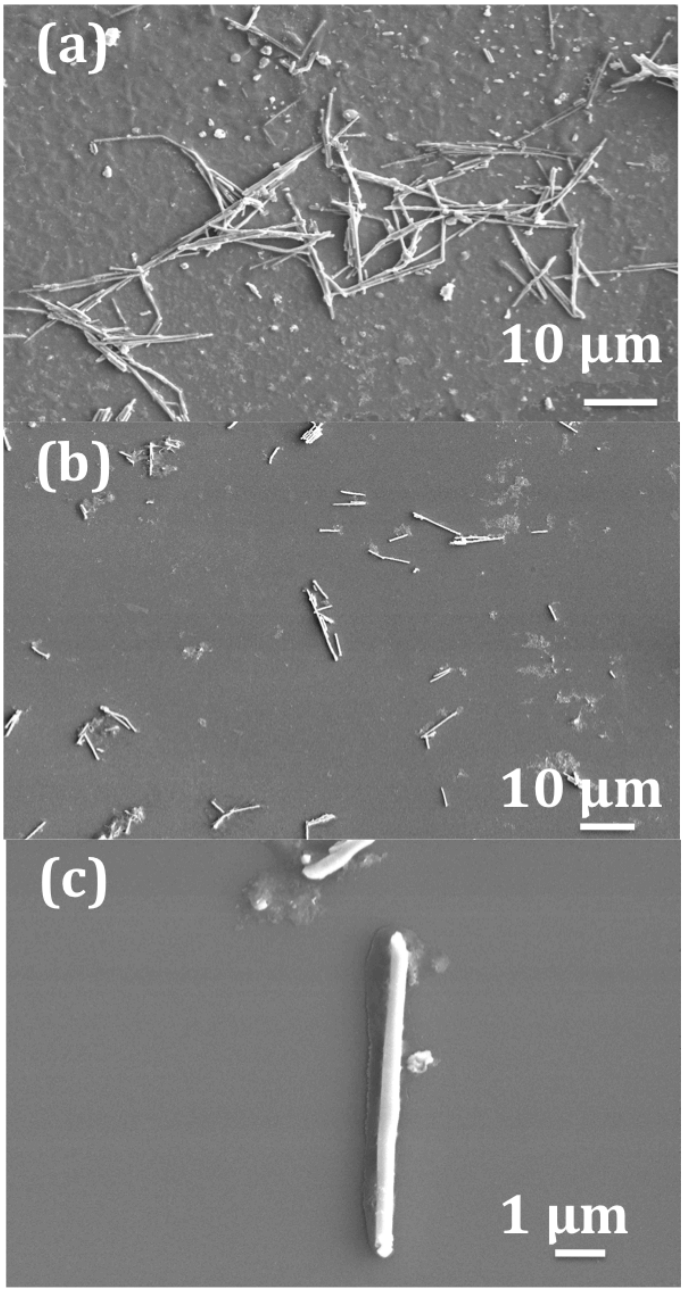

Figure 4.10. Comparison between nanowires dispersed on silicon wafer substrate without adding thiol into ethanol before ultrasonication (a), with thiol added before ultrasonication (b); a single nanowire on substrate surrounded by the thiol is shown in (c).

As is shown in Figure 4.10 (b), with thiol added to the ethanol solution containing copper nanowires before ultrasonication, nanowires spread more uniformly and separately than without adding the thiol in Figure 4.10 (a), where nanowire clusters were formed all over the surface of the substrate. The results demonstrate that with thiol added before ultrasonication, nanowires can spread more uniformly than in ethanol without the thiol, which may benefit future research focused on individual metallic nanowires as electrodes in nanoelectronic devices.

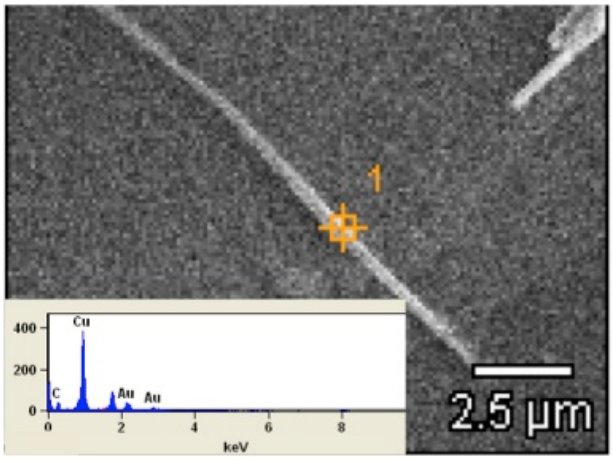

Figure 4.11. EDS spectrum of the as-prepared copper nanowirs.

Elemental analysis of as-prepared copper nanowires, after liberation from AAO templates, was examined by EDS and results are shown in Figure 4.11. It is observed that the nanowires were not extensively oxidized after the template dissolving process based on the absence of oxygen signal. The signals of Au are from the remaining gold coating of the template. The high purity of

copper may be credited to the protection provided by the thiol coating as described above.

A comparison by EDS was conducted to characterize the chemical composition of nanowires being released from templates without adding thiol. From the spectrum in Figure 4.12, the absence of oxygen also demonstrates that no bulk oxidation occurred to the nanowires after template dissolution. Thus, the main role of adding thiol appears to be better isolation to avoid agglomeration on substrates.

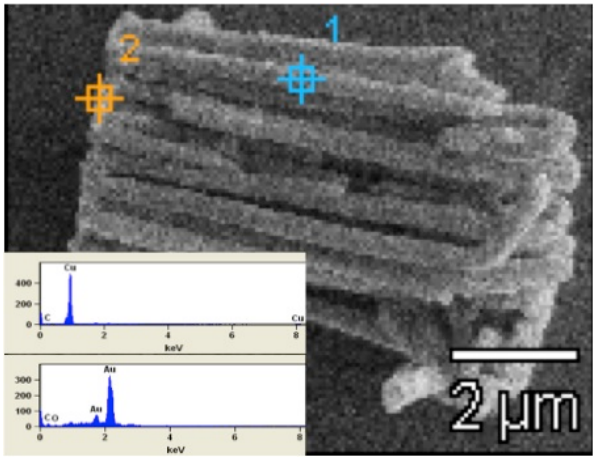

Figure 4.12. EDS spectrum of the copper nanowirs after the dissolution of templates without adding thiol.

4.2.3.3 Changing of Ultrasonicating Time

Refering to the previous results of released nanowires distributed on substrates, it was found that the released nanowires are shorter than then ones embedded in AAO templates. One possibility is that ultrasonication breaks nanowires into smaller segments. In this work, 15 min, 25 min, and 35 min

ultrasonicating time were chosen to disperse nanowires after AAO was dissolved completely.

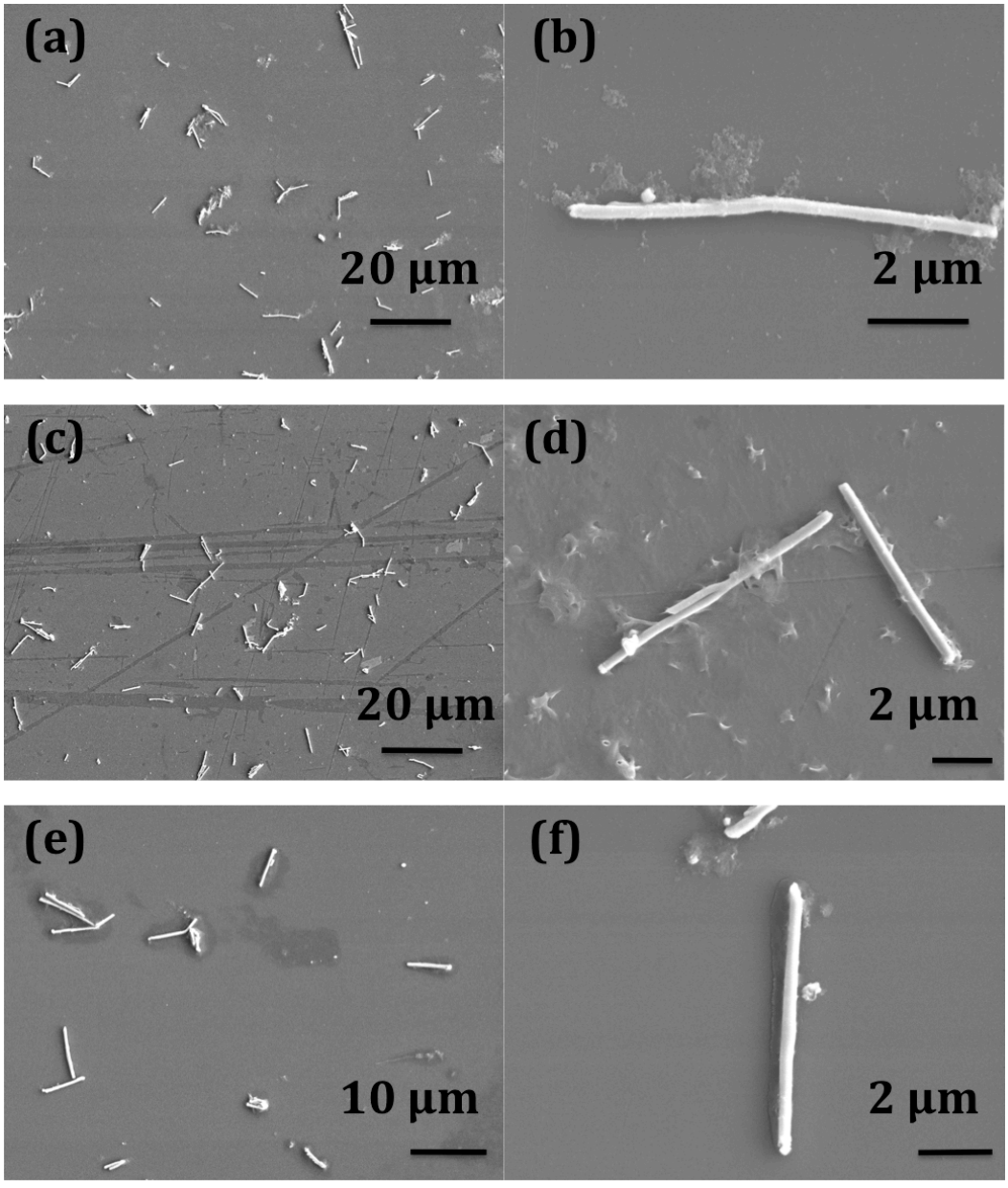

Figure 4.13. Comparison of copper nanowires kept with thiol added dispersed on silicon wafer substrate after various ultrasonication periods. 15 min for (a) and (b); 25 min for (c) and (d); 35 min for (e) and (f).

There is no distinct change among the uniformity of nanowires distributed on the silicon wafer substrate in Figure 4.13 (a), (c) and (e). However, nanowires after 35 min sonication in Figure 4.13 (e) and (f) are shorter than the previous two, which is probably from the sonication process breaking the longer ones into shorter ones. From Figure 4.14, it is found that the density of nanowires dispersed on substrates was not significantly changed, but the length of a selected single nanowire in each case decreased as longer sonicating time was applied. Figure 4.14 shows that the lengths of dispersed nanowires are correlated with the sonicating duration. The length of nanowires were measured by ImageJ via setting the length scale according to the scale bar in Figure 4.13 (b), (d) and (f), and selecting a minimum of 20 nanowires to calculate the average length.

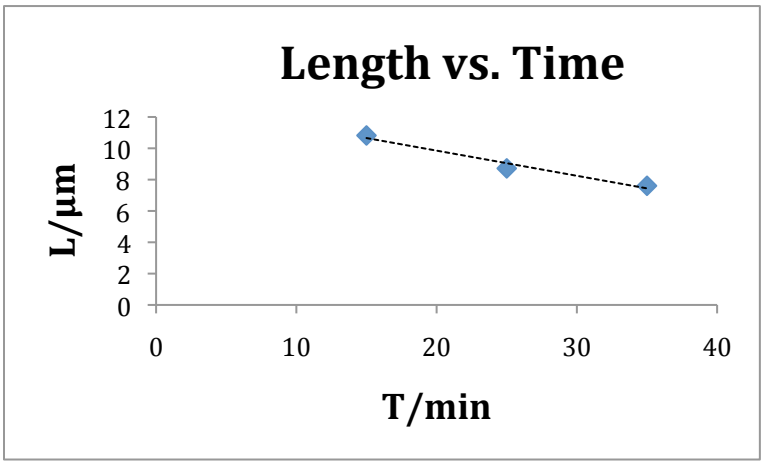

Figure 4.14. Plot of the linear relationship between the varied sonicating time and length of a single-crystal copper nanowire. The line is a guide to the eye.

4.3 Other Single Crystal Metal Nanowires by Electrodeposition

Platinum is one of the most thoroughly researched noble metals as it has potential applications in the fields of biosensors, catalysis, and fuel cells. For example, because of its useful performance toward the detection of hydrogen peroxide, a typical enzymatic product, platinum electrodes have been widely used to immobilize enzymes for the fabrication of biosensors [28].

S.S. Marsha and co-workers [29] have prepared platinum nanowires using similar procedures as used in the synthesis of copper nanowires, including the use of thin Au films as nucleation layers. Electrodepositions were performed using chronoamperometry in 1% (w /w) H_2PtCl_4 solution containing 0.5 M perchloric acid at a potential of 0.35 V (SCE). After deposition, the polycarbonate template was dissolved by immersing the electrode in chloroform [29]. However, the crystallinity of the platinum nanowires was not characterized in this work, and few researchers have synthesized single-crystal platinum nanowires by electrodeposition to date. Table 4.1 presents a review of the experimental conditions of various metallic nanowires, which are all textured with single crystallinity. With further advances in both experiment and theoretical understanding, there is a promising future for controlling the crystalline structure of platinum and other metal nanowires prepared by the template approach.

Table 4.1. Review of experimental conditions and textures of single-crystal metallic nanowires synthesized by template approach. * NW: nanowire.

NW*	Template	Electrolyte	pH	Method	Orientation	Ref.
Ag	AAO	0.2 M $AgNO_3$ and 0.1 M H_3BO_3	Controlled during electrodeposition	Potentiostatic 19 V for 20 nm 40 V for 50 nm	(220)	[30]
Pb	AAO	30 g/L $PbNO_3$ and 45 g/L H_3BO_3	2.5 with nitric acid	Chronoamperometry 2.5 mA/cm^{-2}	(200)	[31]
Bi	AAO	$BiCl_3$ (40 g/L), tartaric acid (50 g/L), glycerol (100 g/L), NaCl (70 g/L), and HCl (1 mol/L)	0.9 with aqueous ammonia (5 mol/L)	Pulsed Potential -1.5 V -1.9 V -1.1 V	(104) (110) (202)	[32]
Au	AAO	Potassium dicyanoaurate(I) Puramet 402 containing 10 g/l of gold	Unknown	Potentiostatic -1.4 V	(110)	[33]
Ni	AAO	0.4 M $NiSO_4.H_2O$, 0.1 M NaCl, 0.1 M H_3BO_3 0.45 M $Na_3C_6H_5O_7{\cdot}2H_2O$	4.0 by adding H_2SO_4 dilute solution	Potentiostatic 2.0 V	(110)	[34]
Sb	AAO	0.02M $SbCl_3$ and $C_{12}H_{25}NaO_4S$	2.0 by 1 M H_2SO_4	Potentiostatic -3.0 V	(012)	[35]

4.4 Molecular Electronic Devices and Single-Crystal Nanowires

According to Moore's Law, the number of transistors that can be placed on an integrated circuit doubles approximately every two years. Rapid miniaturization of microelectronics has led to remarkable increases in computing power while at the same time enabling reductions in cost. To create small structures, a traditional "top-down" approach is employed, in which high device density could be achieved on an integrated circuit using lithography [36]. However, as transistor sizes approach the nanometer scale new issues such as current leakage and excess heat generation emerge and threaten the continuation of Moore's Law. One promising approach to move beyond traditional device scaling is to develop active molecular devices for future

nanoelectronics technologies, an area of study known as molecular electronics or moletronics [37].

Molecules are an appealing choice of electronic components because of their size and adaptability. Because molecules are the smallest stable structures, they can be used as the smallest circuit components. The "bottom-up" approach is based on this idea. In addition, a molecule's electronic behavior can be tailored based on its specific chemistry, such as the addition or removal of functional groups or the presence of reactive environments, allowing the promise of a high degree of control with many chemical options [36].

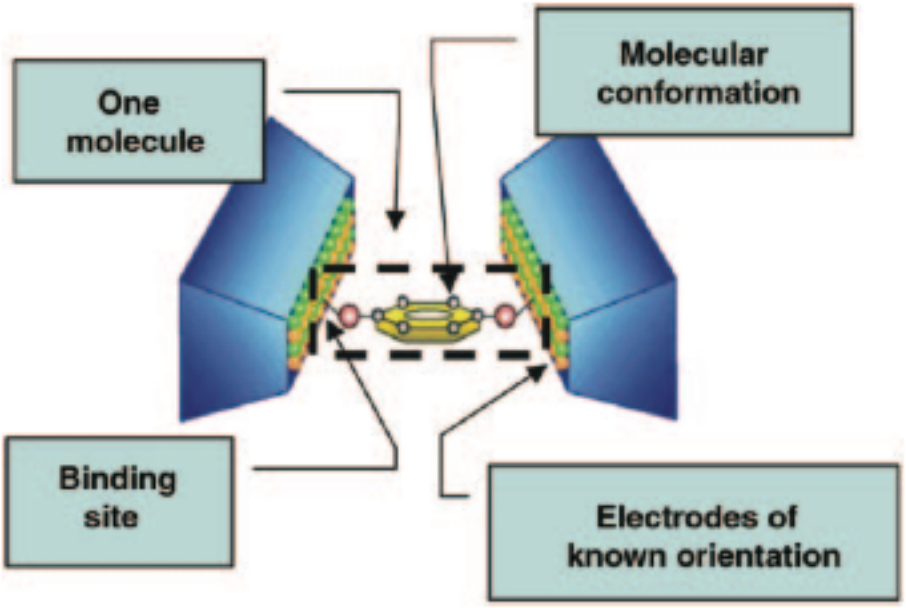

Figure 4.3. A schematic illustration showing a well-characterized molecular junction[38]

The device consisting of a molecular wire bound to two metal electrodes is known as a molecular junction. An electronic transport measurement that is specific to a molecule can be measured when a bias

voltage is applied across a molecular junction. Figure 4.3 is a schematic of an ideal molecular junction for molecular electronic measurements.

Four aspects of a molecular junction that affect conductance have been identified: 1) the geometry of a single molecule bound between two metal electrodes; 2) the molecule itself and its conformation; 3) the binding site at the metal-molecule interface; and 4) the electrode orientation [38].

The electrode's surface morphology, orientation, and composition affect the contact between the metal and molecule, and without understanding the intimate details of electrode structure, an understanding of how these molecular junctions work is incomplete. The techniques demonstrated in this study can be employed to make single-crystal nanowires that may be useful for molecular electronics.

4.5 References

1. Inguanta, R.; Piazza, S.; Sunseri, C., Influence of the electrical parameters on the fabrication of copper nanowires into anodic alumina templates. *Applied Surface Science* **2009,** *255*, 8816-8823.

2. Riveros, G.; Gómez, H.; Cortes, A.; Marotti, R. E.; Dalchiele, E. A., Crystallographically-oriented single-crystalline copper nanowire arrays electrochemically grown into nanoporous anodic alumina templates. *Applied Physics A* **2004,** *81*, 17-24.

3. Toimil-Molares, M. E.; Buschmann, V.; Dobrev, D.; Neumann, R.; Scholz, R.; Schuchert, I. U.; Vetter, J., Single-crystalline copper nanowires produced by electrochemical deposition in polymeric ion track membranes. *Adv Mater* **2001,** *13*, 4.

4. Toimil-Molares, M. E.; Brotz, J.; Buschmann, V.; Dobrev, D.; Neumann, R.; Scholz, R.; Schuchert, I. U.; Trautmann, C.; Vetter, J., Etched heavy ion tracks in polycarbonate as template for copper nanowires. *Nucl Instrum Meth B* **2001,** *185*, 192-197.

5. Mohl, M.; Pusztai, P.; Kukovecz, A.; Konya, Z.; Kukkola, J.; Kordas, K.; Vajtai, R.; Ajayan, P. M., Low-Temperature Large-Scale Synthesis and Electrical Testing of Ultralong Copper Nanowires†. *Langmuir* **2010,** *26*, 16496-16502.

6. Gao, T.; Meng, G. W.; Zhang, J.; Wang, Y. W.; Liang, C. H.; Fan, J. C.; Zhang, L. D., Template synthesis of single-crystal Cu nanowire arrays by electrodeposition. *Applied Physics A Materials Science & Processing* **2001,** *73*, 251-254.

7. Tian, M. W., J.; Kurtz, J.; Mallouk, T. E.; Chan, M. , Electrochemical Growth of Single-Crystal Metal Nanowires via a Two-Dimensional Nucleation and Growth Mechanism. *Nano Lett* **2003,** *3*, 5.

8. Vitos, L. R., A.V.; Skriver, H.L.; Kollar, J., The surface energy of metals. *Surface Science* **1998,** *411*, 7.

9. Sun, H.; Yu, Y.; Li, X.; Li, W.; Li, F.; Liu, B.; Zhang, X., Controllable growth of electrodeposited single-crystal nanowire arrays: The examples of metal Ni and semiconductor ZnS. *Journal of Crystal Growth* **2007,** *307*, 472-476.

10. Duan, J.; Liu, J.; Mo, D.; Yao, H.; Maaz, K.; Chen, Y.; Sun, Y.; Hou, M.; Qu, X.; Zhang, L., Controlled crystallinity and crystallographic orientation of Cu nanowires fabricated in ion-track templates. *Nanotechnology* **2010,** *21*, 365605.

11. Pan, H.; Sun, H.; Poh, C.; Feng, Y.; Lin, J., Single-crystal growth of metallic nanowires with preferred orientation. *Nanotechnology* **2005,** *16*, 1559-1564.

12. Gao, T.; Meng, G. W.; Wang, Y. W.; Sun, S. H.; Zhang, L., Electrochemical synthesis of copper nanowires. *J Phys-Condens Mat* **2002,** *14*, 355-363.

13. Thongmee, S.; Pang, H. L.; Ding, J.; Lin, J. Y., Fabrication and magnetic properties of metallic nanowires via AAO templates. *Journal of Magnetism and Magnetic Materials* **2009,** *321*, 2712-2716.

14. Serre, C. Y., N.; Martınez, S.; Perez-Rodrıguez, A.; Morante, J.R.; Esteve, J.; Montserrat, J. , Electrochemical deposition of Cu and Ni/Cu multilayers in Si Microsystem Technologies. *Sensors and Actuators A: Physical* **2005,** *123-124*, 633-639.

15. Diao, J.; Gall, K.; Dunn, M., Surface stress driven reorientation of gold nanowires. *Phys Rev B* **2004,** *70*.

16. Wang, X. W.; Fei, G. T.; Xu, X. J.; Jin, Z.; Zhang, L. D., Size-dependent orientation growth of large-area ordered Ni nanowire arrays. *J Phys Chem B* **2005,** *109*, 24326-30.

17. Sander, M. S. G., R.; Sands, T.; Stacy, A. M. , Structure of Bismuth Telluride Nanowire Arrays Fabricated by Electrodeposition into Porous Anodic Alumina Templates. *Chemical Materials* **2003,** *15*, 5.

18. Guo, D. Z., M.; Jin, Z; Kang, R., Effects of Chloride Ion on the Texture of Copper and Cu-ZrB2 Coatings Electrodeposited from Copper Nitrate Solution in Different Plating Modes. *Journal of materials science and technology* **2006,** *22*, 4.

19. Shao, W.; Pattanaik, G.; Zangari, G., Influence of Chloride Anions on the Mechanism of Copper Electrodeposition from Acidic Sulfate Electrolytes. *J Electrochem Soc* **2007,** *154*, D201.

20. Xu, Q. M., G.; Wu, X.; Wei, Q.; Kong, M.; Zhu, X.; Chu, Z, A Generic Approach to Desired Metallic Nanowires Inside Native Porous Alumina Template via Redox Reaction. *Chemistry of Materials* **2009,** *21*, 6.

21. Schonenberger, C. v. d. Z., B. M. I.; Fokkink, L. G. J.; Henny, M.; Schmid, C.; Kruger, M.; Bachtold, A.; Huber, R.; Birk, H.; Staufer, U., Template synthesis of nanowires in Porous Pplycarbonate Memberanes: Electrochemistry and Morphology. *Journal of Physical Chemistry B* **1997,** *101*, 9.

22. Mohapatra, S. K. G., T.; Misra, M.; Raja, K.S. , Electrodeposition of Al-Sb Nanowire Arrays for Radiation Detection. In *MPMD 7th Global Innovations Proceedings: Trends in Materials R&D for Sensor Manufacturing Technologies*, The Minerals, Metals & Materials Society: 2006; p 8.

23. Gupta, M. K., V.; Spivey, J. J. , Electrodeposition of Cu-ZnO and Mn-Cu-ZnO Nanowires/tubes for Synthesis of Ethanol. In *214th ECS Meeting*, ECS: MA, 2008; Vol. Abstract #281.

24. Schwanbeck, H. S., U., Preparation and characterisation of magnetic nanostructures using filtration membranes. *Electrochimica Acta* **2000,** *45*, 10.

25. Leo, M. D. P., F. C.; Moretto, L. M.; Scopece, P.; Polizzi, S.; Ugo, P., Towards a Better Understanding of Gold Electroless Deposition in Track-Etched Templates. *Chemical Materials* **2007,** *19*, 10.

26. Martin, C. R. N., M.; Jirage, K.; Kang, M., Investigations of the Transport Properties of Gold Nanotubule Membranes. *Journal of Physical Chemistry B* **2001,** *105*, 10.

27. Gelves, G. A.; Sundararaj, U.; Haber, J. A., Electrostatically Dissipative Polystyrene Nanocomposites containing Copper Nanowires. *Macromolecular Rapid Communications* **2005,** *26*, 1677-1681.

28. Yang, M.; Qu, F.; Lu, Y.; He, Y.; Shen, G.; Yu, R., Platinum nanowire nanoelectrode array for the fabrication of biosensors. *Biomaterials* **2006,** *27*, 5944-50.

29. Mahshid, S. S. D., A.; Hashemi D. S.; Ghorbani, M.; Ghahramaninezhad, A. , Electrodeposition of Platinum Nanowires: Electrochemical Characterization. *ECS Transactions* **2010,** *28*, 11.

30. Zhang, J.; Wang, X.; Peng, X.; Zhang, L., Fabrication, morphology and structural characterization of ordered single-crystal Ag nanowires. *Applied Physics A: Materials Science & Processing* **2002,** *75*, 485-488.

31. Pang, Y. T. M., G. W.; Zhang, L. D.; Shan, W. J.;Gao, X. Y.; Zhao, A. W.; Mao, Y. Q. , Arrays of ordered Pb nanowires with different diameters in different areas embedded in one piece of anodic alumina membrane. *Journal of Physics: Condensed Matter* **2002,** *14*, 9.

32. Zhu, Y.; Dou, X.; Huang, X.; Li, L.; Li, G., Thermal properties of bi nanowire arrays with different orientations and diameters. *J Phys Chem B* **2006,** *110*, 26189-93.

33. Karim, S.; Toimil-Molares, M. E.; Maurer, F.; Miehe, G.; Ensinger, W.; Liu, J.; Cornelius, T. W.; Neumann, R., Synthesis of gold nanowires with controlled crystallographic characteristics. *Applied Physics A* **2006,** *84*, 403-407.

34. Yue, G.; Xu, Q.; Meng, G.; He, X.; Han, F.; Zhang, L., Electrochemical synthesis and magnetic properties of single-crystal and netlike poly-crystal Ni nanowire arrays. *Journal of Alloys and Compounds* **2009,** *477*, L30-L34.

35. Chen, Y.; Yang, Y.; Chen, X.; Liu, F.; Xie, T., Orientation-controllable growth of Sb nanowire arrays by pulsed electrodeposition. *Materials Chemistry and Physics* **2011,** *126*, 386-390.

36. Maruccio, G.; Cingolani, R.; Rinaldi, R., Projecting the nanoworld: Concepts, results and perspectives of molecular electronics. *J Mater Chem* **2004,** *14*, 542.

37. Hsu, I. Characterization of ALD Copper Thin Films on Palladium Seed Layers For Molecular Electronics. University of Delaware, Newark, 2008.

38. Hersam, M. C. R., R. G., Charge Transport Through Molecular Junctions. *Mrs Bull* **2004**, 6.